PCCP

Origins and Properties of the Tetrel Bond

Journal:	*Physical Chemistry Chemical Physics*
Manuscript ID	CP-PER-01-2021-000242.R1
Article Type:	Perspective
Date Submitted by the Author:	16-Feb-2021
Complete List of Authors:	Scheiner, Steve; Utah State University, Department of Chemistry and Biochemistry

Origins and Properties of the Tetrel Bond

Steve Scheiner*

Department of Chemistry and Biochemistry
Utah State University
Logan, Utah 84322-0300
steve.scheiner@usu.edu

Abstract

The tetrel bond (TB) recruits an element drawn from the C,Si,Ge,Sn,Pb family as electron acceptor in an interaction with a partner Lewis base. The underlying principles that explain this attractive interaction are described in terms of occupied and vacant orbitals, total electron density, and electrostatic potential. These principles facilitate a delineation of the factors that feed into a strong TB. The geometric deformation that occurs within the tetrel-bearing Lewis acid monomer is a particularly important issue, with both primary and secondary effects. As a first-row atom of low polarizability, C is a reluctant participant in TBs, but its preponderance in organic and biochemistry make it extremely important that its potential in this regard be thoroughly understood. The IR and NMR manifestations of tetrel bonding are explored as spectroscopy offers a bridge to experimental examination of this phenomenon. In addition to the most common σ-hole type TBs, discussion is provided of π-hole interactions which are a result of a common alternate covalent bonding pattern of tetrel atoms.

Keywords: electron density, σ-hole; monomer deformation; substituent effect; IR; NMR

INTRODUCTION

Recent years have witnessed a renaissance of the study of noncovalent bonds. Of particular interest has been the series of bonds that are close analogues of the textbook H-bond (HB). The replacement of the bridging proton by a member of the halogen family yields a so-called halogen bond (XB) of comparable strength, and sharing many of the same characteristics as a HB. It has also been increasingly recognized that XBs are not alone, and that similar phenomena occur when the bridging atom is a member of neighboring families of the periodic table, within the correspondingly named chalcogen (YB) and pnicogen (ZB) bonds. The tetrel family begins with the electronegative nonmetal C, then moves on to semimetals Si and Ge, after which it includes the Sn and Pb metals, so is highly diverse in this regard. Nonetheless, all of these atoms have been shown to be capable of engaging in a tetrel bond (TB), similar to the other types mentioned above. The TB is defined for our purposes as an attractive interaction in which a tetrel atom serves as electron acceptor in a Lewis acid, to an electron-donating Lewis base.

As a summary history of this phenomenon, one of the earliest observations of what later came to be known as a tetrel bond arose when Mani and Arunan [1] recognized that placement of an electron-withdrawing substituent on methane produced an electron-deficient site on the opposite face of the tetrahedron. This positive site could then interact attractively with any of a variety of nucleophiles such as H_2O in what these authors referred to as a carbon bond. This idea was soon generalized to the entire C-family, under the rubric of tetrel bond, when Bauzá et al found evidence [2] of close contacts between Si, Ge, and Sn with O or halogen-containing bases in a survey of the CSD. Quantum calculations in model systems containing a bifurcated arrangement with two T atoms interacting directly with a neutral OH_2 or halide verified the presence of a strong interaction. Note that the T atoms considered did not include C, which foreshadows this atom occupying a special place in this field, as discussed below. When the C atom is surrounded by several electron-withdrawing atoms, as in $ArCF_3$, where Ar represents an aryl group, it seems able to participate in such a bond, as indicated by follow-up work by this same group [3], although this capability was undoubtedly reinforced by the use of an anion as base. Mani and Arunan amplified on the participation by Me in a TB [4] wherein a series of RMe molecules formed such a bond with the small π-donors ethylene and acetylene.

C was included in the set of TF_4 acids considered by Donald and Tawfik [5], who also extended the list to Pb. A number of trends emerged from the data that are common with other related noncovalent bonds such as halogen, chalcogen, and pnicogen bonds. The lightest C atom was reluctant to engage in TBs, as the bond strengthened quickly from Si to Sn, where it plateaued on going up to Pb. In fact, while all studies confirm the reduced ability of C to engage in TBs, there remains some controversy as to the order of the others. Liu et al [6] found the strength diminishes in the order Sn > Si > Ge and Grabowski observed Pb to be inferior to its lighter Sn counterpart [7]. Another study [8] found near equivalence of Si and Ge. In spite of its general reluctance to engage in tetrel bonds with any strength, the methyl group does so when paired with a halide [9], as observed from both a computational and a crystal survey perspective.

Grabowski [10] showed that replacing some of the F atoms of TF_4 by H reduced its propensity to engage in a TB, in part by reducing the depth of the σ-hole. The author also fortified the idea that charge transfer, in particular that from the base lone pair to the σ* antibonding orbital of the acid, represents an important component of these bonds, as well as the usefulness of AIM, again amplifying the commonalities with other noncovalent bonds. The lowering effect of TB formation upon the internal vibrational frequency, as well the intensification of this band, was noted, adding to the similarities between the TB and HB. Grabowski also suggested that the formation of a TB is in some sense a predecessor of the full S_N2 reaction that involves a central T atom.

Experimental confirmation of the existence of TBs continues to emerge. The microwave spectrum of the SiH_4/H_2O pair [11] verified the appropriate geometry. Upon difluorination, the methyl group forms strong enough tetrel bonds as to persist in the gas phase where its structure can be elucidated by microwave spectra [12] which have verified the tetrel bond [13] between CO_2 and the O atom of formamide, to the N of an amine [14]or the O of ketones [15]. Franconetti and Frontera [16] identified a number of crystals with tetrel bonds involving Pb(IV), which were verified by quantum calculations. Pb··N tetrel bonds may be fairly common [17], and situations have been uncovered wherein the four covalently bonded ligands all lay in the same Pb hemisphere [18].

The present article consists of a tour of the current field of tetrel bonds. The first section explains in some detail the fundamental underpinnings at their most elementary level. The next section discusses certain aspects of the TB that distinguish it from its closely related cousins, such as the H-bond and the halogen bond. Within the regime of atoms that can engage in a TB, the first-row C atom is a reluctant participant. The next section thus explores this reluctance and the circumstances under which it can be circumvented. Within the means by which experimentalists might explore and quantify TBs, IR and NMR spectroscopy stand out as perhaps the most useful, given their success in understanding the H-bond. The next section thus opens a dialogue based on quantum calculations as to what spectroscopists might expect as they probe this question. The last section offers a brief tour of other aspects of TBs, including π-bonds, cooperativity, and charge assistance.

UNDERLYING PRINCIPLES

The roots of the tetrel bond are discussed here in the context of T=Ge as an example. The replacement of one of the H atoms of GeH_4 by an electron-withdrawing F atom illustrates some of the fundamental underpinnings of the tetrel bond. (Specific data described below were computed at the M06-2X/aug-cc-pVDZ level.) These effects begin with the T-X bonding orbital, as elucidated by the NBO localization procedure, which is pictured in Figs 1a and 1b for GeH_4 and $GeFH_3$, respectively. Attention is focused on the right side of the Ge atom where an incoming base would approach to eventually engage in a TB with Ge. In either case, this orbital has a great deal more density to its left, toward the H or F atom, than to its right. And this

displacement is amplified for F. The replacement of H by F reduces the size of the red lobe of this σ bonding orbital to the right of Ge by sucking density away toward the F atom.

This orbital shift has a number of implications. In the first place, the leftward shift of this σ(GeX) orbital depletes some density from the area to its right, leaving what is sometimes called a polar flattening or σ-hole [19-26]. The broken lines in Fig 2a indicate the electron density associated with this particular orbital along a line emanating from the central Ge atom, and pointing to the right, directly away from the X substituent. Of course this density drops as R increases in both cases as one moves away from Ge. More importantly, the downward displacement of the blue curve with respect to the black one demonstrates the loss of density arising from the H→F substitution is substantial, and increases as one moves closer to the Ge atom. The solid curves represent the total electron density of the entire molecule in the same region. These totals are of course larger than the partial densities of a single orbital. But the same trends persist. Replacement of the H by F drops the electron density, and by almost the same amount as it reduces the density attributed to the single σ(GeX) orbital.

This reduced density in the substituted system allows a base to approach more closely to the central Ge atom before being overcome by exchange repulsion. Arbitrarily choosing a total density of 0.0002 au as the maximum that the base can overpower, this critical density would be reached for R=2.65 Å for GeH_4 while $GeFH_3$ would permit a base to come some 0.20 Å closer. So the density-depleted σ-hole is partially responsible for permitting the shorter intermolecular distances typically seen in stronger TBs.

The anisotropy of the total electron density is exhibited in Fig 2b, as a function of θ, the deviation of the point of reference from the X-Ge bond extension. This density has its minimum along this extension at θ=0, again consistent with the extraction of density by the X-Ge σ-bond along its axis and the ensuing σ-hole. The density climbs more quickly in the positive θ direction as this displacement brings the reference point closer to the electron cloud associated with the H atom. Note also that the density for the fluorosubstituted molecule is uniformly smaller than that for GeH_4, an angular manifestation of the density shifts caused by F.

This H→F substitution has additional implications for a potential tetrel bond. The depletion of electron density from the region opposite the F atom leads to an increase in the positive electrostatic potential. This positive region is commonly referred to as a σ-hole (although strictly speaking this term refers to the hole in the density) and is illustrated by the blue regions in Figs 3a and 3b on an envelope surrounding each molecule. If one considers a particular surface, that on which the electron density is 0.001 au, the maximum values of the molecular electrostatic potential (MEP) for GeH_4 and $GeFH_3$ are equal to 0.028 and 0.069 au, respectively. The higher V_{max} for the fluorosubstituted Lewis acid would be better able to draw in the negative potential of an approaching nucleophile.

However, this particular surface is somewhat arbitrary. The maximum on this surface lies some 2.10 Å from the Ge of GeH_4, and only 1.98 Å from $GeFH_3$, different from one another, and both quite a bit closer than a nucleophile can approach within a TB complex. It might thus be sensible to examine the MEP along a broader range of R, the distance from Ge. This behavior is

exhibited in Fig 4a where it may be seen first that the MEP becomes more positive as one approaches the Ge nucleus, fully in keeping with the reduced shielding experienced from the surrounding electrons. More importantly, the MEP of $GeFH_3$ is quite a bit more positive than is that of the unsubstituted GeH_4 for all distances. The difference is not exactly uniform, varying between 0.014 au for R=3.5 Å up to 0.033 au for R=2 Å. But also when one considers that the lower electron density of $GeFH_3$ permits the closer approach of a base, this difference is amplified. For example, the optimized R(Ge··N) distance in the tetrel-bonded $H_4Ge··NH_3$ complex is 3.16 Å, at which point the MEP of H_4Ge would be 0.0043 au. This MEP is 7 times smaller than the 0.0297 au for $FH_3Ge··NH_3$ at its equilibrium distance of 2.71 Å.

The anisotropy of the MEP may be plainly seen in Fig 4b, derived at a distance of 3 Å from the Ge atom. The maximum lies directly along the X-Ge axis, θ=0, and then tails off in either direction. In addition to the larger MEP for FH_3Ge than for H_4Ge at θ=0, 0.023 vs 0.005 au, another measure of the depth of the σ-hole is the difference in MEP between θ=0 and a larger θ such as 50°. This difference is 0.010 au for FH_3Ge as compared to only 0.006 au for H_4Ge.

There is a further effect of the substitution of an electron-withdrawing agent on the Lewis acid that derives directly from the σ*(GeX) antibonding orbital into which density is transferred from the lone pair of the approaching nucleophile. As X becomes more electronegative, the energy of this antibonding orbital will drop down. For example, the energy of this orbital is 0.246 and 0.133 au for GeH_4 and $GeFH_3$, respectively. The reduction in its energy brings it down closer to that of the nucleophile lone pair orbital with which it interacts. Perturbation theory places the energy difference between the two interacting orbitals in the denominator of the expression of the energetic consequence of this transfer, so the charge transfer energy ought to rise as the antibonding orbital energy drops down. Again using the TBs formed between GeH_4 and $GeFH_3$ as our example, the NBO second-order perturbation energy for the former is equal to 4.3 kcal/mol, which is amplified to 12.7 kcal/mol for the latter. Of course, part of this difference is a consequence of the closer approach of the two subunits in $FH_3Ge··NH_3$. However, even if the latter is forced to adopt the same 3.16 Å separation as is found in $H_4Ge··NH_3$, E(2) remains larger for the fluorosubstituted system, due to the smaller energy difference between the pertinent orbitals.

Trends in Tetrel Bond Strength

With the preceding as a basis, it becomes easier to understand the trends that have emerged in the literature concerning tetrel bonds. High electron-withdrawing capacity of a substituent accentuates the various effects, and thus strengthens any incipient TB. Adding multiple such electronegative substituents will also have a positive effect, even if the replacement in question does not lie directly opposite the site in question. These other substituents will amplify the depth of the σ-hole. For example, replacing two more H atoms of FH_3Ge by F enhances the σ-hole depth from 0.069 to 0.083 au. The interaction energy with a NH_3 base is thereby increased from 8.50 for FH_3Ge to 22.41 kcal/mol with the extra two F atoms.

With respect to the particular T atom, as one moves up the group 14 column of the periodic table, these atoms become less electropositive and polarizable. Both of these factors mitigate the depth of the σ-hole and thus weaken a TB. As an example, replacing the Ge atom of FH_3Ge by the lighter C reduces the σ-hole depth in half from 0.069 to 0.031 au. This substitution also reduces the charge transfer energy that would accrue from a base by raising the σ*(TF) antibonding orbital energy from 0.133 to 0.297 au. The net result is a drop in the TB energy down to only 2.16 kcal/mol. This weakening is also reflected in the equilibrium separations. In comparison to the TB length R(Ge··N) of 2.708 Å in $FH_3Ge··NH_3$, this distance elongates to 3.064 Å when Ge is replaced by C. In fact, it is this sensitivity of the TB to the nature of the T atom that raises the question as to whether and under what conditions a C atom might participate in such a bond, a topic which is discussed in more detail below.

These trends may be envisioned more systematically for four tetrel atoms ranging from C to Sn, and with various degrees of fluorosubstitution for each. The binding energy E_b of each with NH_3 as base was calculated [27] at the MP2/aug-cc-pVDZ level (using the relativistic aug-cc-pVDZ(PP) pseudopotential for Sn) and corrected for basis set superposition error by the counterpoise procedure. The base was situated opposite the H atom of TH_4 and F_3TH, while it lies opposite to the F atom in FTH_3 and F_4T. This distinction is stressed in the respective σ_H or σ_F designations in Table 1. One can see from the table that the binding energy is quite small until F atoms are added, after which it rises rapidly with each new addition of F. The increase with size of T atom is also apparent. The reluctance of C to engage in TBs is visible in the first row of Table 1. These trends have some small "hiccups". For example, the binding energy of GeH_4 is slightly smaller than that of SiH_4. And adding two more F atoms to FTH_3 leads to a minor drop, but this can be attributed to switching from a σ_F to σ_H hole where the subscript indicates the atom directly opposite the nucleophile position. With regard to the actual depths of the σ-holes in the MEP, these quantities are displayed in Table 2, and reflect the energetic trends of Table 1 quite well, deepening for larger T atoms. The shallower σ-holes for F_3TH as compared to FTH_3 reflect the switching from σ_F hole to σ_H.

The properties of a base of course also play a role in the interaction with the tetrel-containing Lewis acid. A stronger base, with a more available lone pair, will engage in the strongest TBs. This ability is aided when electron-releasing substituents such as alkyl groups are placed on the electron-donating atom. Besides electrostatics and charge transfer effects, London dispersion can make a significant contribution as well. This component will increase along with the size and polarizability, of the central tetrel atom, and will be amplified as well by larger substituents on both the acid and base units. It should be noted that the principles outlined above are not limited only to tetrel bonds. They apply equally to the closely related pnicogen, chalcogen, and halogen bonds, where the central tetrel atom is replaced by one from each of these families of elements.

MONOMER DEFORMATION

There are certain characteristics that differentiate to some degree the tetrel bond from the related halogen and other σ-hole bonds. Perhaps the most important of these is related to steric repulsions and monomer deformation. If one considers the idealized case of sp^3 hybridization of the central atom, then the σ-hole that lies directly opposite one of these bonds will be situated some 70° from the other three bonding pairs. In the case of a halogen atom, these three pairs will all be nonbonding lone pairs. But as one progresses to chalcogen and pnicogen, first one and then two of these sites are occupied by substituents. An incoming base may successfully avoid steric repulsion with these substituents by moving away from them, and toward the substituent that is inducing the σ-hole. But no such dodging is possible for a tetrel atom, as all three of the sites are occupied by a substituent. The only way to minimize the steric repulsions is for these three substituents to move away from the incoming nucleophile, much as do the spokes of an umbrella when it opens. This displacement away from an idealized tetrahedral arrangement leads to a good deal of deformation energy within the Lewis acid monomer, much more than is encountered in halogen, chalcogen, or pnicogen bonds.

Geometrical deformations are part and parcel of tetrel bonding [28-30]. One early study that noted this fact considered tetrel-bonded complexes of $H_nF_{4-n}Si$ with a N-base [31], and another [32] pointed out the deformation of TBs are much larger than in pnicogen, chalcogen, or halogen bonds. The addition of two N bases to a tetrahedral SnR_4 system takes the complex to an octahedral shape, and this octahedron can bind a Cl^- [33].

Some measure of this deformation effect can be drawn again from the series of complexes of fluorosubstituted TH_4 with NH_3 [27]. The top half of Table 3 documents the changes in the "umbrella angle" defined as that between the F (or H) atom opposite the NH_3, and the other atoms. In the two cases on the left, TH_4 and FTH_3, the atoms that must move aside to make room for the approaching base are H. Their small size requires only minor motions, 5° or so, even less for TH_4. But when the substituents obstructing the entry of the nucleophile are the larger F atoms, the umbrella angle drops by some 11°-13° in order to accommodate the incoming NH_3. These monomer distortions raise the energy of the monomer by an amount commonly termed the deformation energy E_{def}. As listed in the lower half of Table 3, these energies are negligible for TH_4 and rise to less than 2 kcal/mol for FTH_3. But again, the large-scale opening of the umbrella required for F_3TH and F_4T leads to quite large deformation energies, up to 20 kcal/mol in some cases. Notice also that these deformation energies are largest for the small Si atom, then diminishing as T grows in size, even though the umbrella angle changes are about the same for all.

There is an important issue that arises when the deformation energy is substantial as in some of these cases. The interaction energy E_{int} is usually conceived in terms of a "pure" interaction, between the two subunits when they are in the geometries they adopt within the complex. But the actual reaction energy, commonly denoted the binding energy E_b, takes one to the product complex from the reactants before they undergo any structural changes, i.e. in their fully optimized geometries. This entire reaction process thus consists of two conceptual steps. The

two monomers first rearrange to the geometries they will adopt within the complex (E_{def}), after which they interact with one another (E_{int}), as expressed by Eq (1)

$$E_b = E_{int} + E_{def} \quad (1)$$

In cases where E_{def} is appreciable, as in some of the systems in Table 3, the binding energy can be quite a bit less exothermic than is E_{int}. One must therefore be careful to distinguish between these two quantities when evaluating the strength of a tetrel bond, or any other with significant monomer distortion.

Of course, not all of the substituents surrounding a central tetrel atom will generally be single atoms like H or F. The influence of larger size substituents was considered [34] for a series of FTR_3 molecules in which the F created the σ-hole to which the base was attracted. A series of progressively larger R substituents was considered, ranging from atoms H, Cl, Br, and I up to CH_3, CF_3, isopropyl, and t-butyl groups. Table 4 presents the relevant energetic data for the complexes formed between NH_3 and the various Lewis acids containing Si as its central T atom. When the three H atoms of $FSiH_3$ are replaced by methyl groups, the ensuing crowding forces the NH_3 out much further from the Si to the point where the Si··N TB is replaced by weak HBs to the methyl H atoms. Replacing one of these methyl groups by the electron-withdrawing CF_3 restores the tetrel bond, and pulls the N in quite a bit closer. The interaction energy climbs up to 13.15 kcal/mol. However, in forming this TB, the acid is deformed to the tune of 11 kcal/mol. So although the interaction energy of $FSiMe_2(CF_3)$ is nearly double that of $FSiH_3$, its binding energy is cut in half. The next row of Table 4 shows that replacing a second methyl group by CF_3 nearly doubles the interaction energy, while also raising the deformation energy. Because the former increase is larger than the latter, the resulting binding energy increases from 2 to 9 kcal/mol. Very similar increases occur when a third CF_3 group is added.

The isobutyl group (Iso) is considerably larger than methyl, without the benefit of enhancing the σ-hole on the Si atom as would an electron-withdrawing group. It offers the same sort of steric obstruction as do the three methyl groups but if the NH_3 can sneak inside them it can engage in a tetrel bond with the Si. However, the deformation energy is such that it overwhelms the interaction energy, making this bonding process an endothermic one. This problem is partially alleviated if one of these isobutyl groups is replaced by CF_3. The same sort of steric repulsion issues plague the tert-butyl (Tb) groups where the TB is negated by the high deformation energy. Atoms larger than H and F present steric problems. The high deformation energies involved in tetrel bonding to SiX_3 are somewhat smaller than the interaction energies for X= Cl, Br, or I, so the resulting E_b is negative, i.e. exothermic.

The entries in Table 5 indicate a reduction in the deformation energies for T atoms larger than Si. These quantities are less than 7 kcal/mol for the most part. This effect is easily visible for the particularly bulky t-butyl substituents. From the 17.4 kcal/mol deformation energy for $FSiTb_3$, this quantity drops to 12.7, 6.4, and 2.9 kcal/mol, respectively, as the T atom enlarges to Ge, Sn, and finally to Pb. When combined with the reasonably large interaction energies, this

diminishing deformation energy permits the overall binding energy to switch from endothermic to exothermic for the two larger T atoms. In summary, then, the deformation energies are rather substantial for these larger substituents, so exert a profound effect upon the overall energetics of the binding process. In many cases, the deformation greatly reduces the exothermicity, but in some cases it is large enough to reverse the energetics to make it endothermic.

Another implication of deformation energy arises in the context of the geometry adopted by the complex. When a base like pyridine approaches a TF_4 molecule, the latter will deform [35] into a trigonal bipyramid, from which the base can choose either an axial or equatorial site. The interaction energy favors the equatorial site by a wide margin. But this consideration is outweighed by the much larger deformation energy for this configuration, so that it is the axial position which is ultimately preferred.

Secondary Effects of Monomer Distortion

As we have seen above, as the base approaches its target tetrel atom on the Lewis acid the substituents on the latter tend to bend back away from the base to minimize steric repulsions. This deformation has a direct energetic cost which reduces the overall exothermicity of the complexation process. But there are less direct secondary issues as well. As a prime example, it was discussed above how the positive area of the MEP that lies along the extension of a R-T bond, termed a σ-hole, acts to draw in the nucleophile. But one must understand that the opening up of the umbrella around the T atom might cause a change in the depth of this σ-hole.

These ideas were explored in the context of fully fluorosubstituted TF_4 molecules [36] which were allowed to interact with three different N-bases of varying strength. The NCH unit with its sp-hybridization is the weakest such base, and as such its interaction energy with the TF_4 acids is the lowest, as may be seen in the first three rows of Table 6. NH_3 is a bit stronger than is pyrazine, as reflected in the remaining entries. For each base, the interaction energies climb along with the size of the central T atom from Si to Ge to Sn. Note that these quantities cover a wide range from less than 3 kcal/mol for $HCN\cdots SiF_4$, up to 35 kcal/mol for those involving SnF_4.

The next column of Table 6 displays the deformation energies which very roughly parallel the interaction energies in the sense that the deformation is smallest for the weak NCH base, and larger for the other two bases. For the latter two, the deformation energy declines as T grows in size, reproducing the common pattern noted earlier. The opposite trend is noted for NCH, though. This distinction can be traced to the high sensitivity of the interaction energy to T which is in turn reflective of the dramatic changes in intermolecular distance. The R(T··N) distance drops precipitously from 3.115 Å for Si down to 2.366 Å for Sn. This much closer approach of the NCH for the larger T atoms induces a correspondingly larger geometric distortion within the acid, which is mirrored in E_{def}. When incorporated into Eq (1) above, the overall reaction energies E_b are exothermic in all cases, and reflect the growing tetrel bond strength associated with both stronger base and larger T.

One can inquire into the implications of the monomer deformation in a number of ways. First, suppose that the Lewis acid monomers had been frozen in their fully optimized tetrahedral

structures, without the ability for the three umbrella spokes to open as the base approaches. The interaction energies calculated under this frozen condition are reported in the first column of Table 7 as $E_{int}(f)$. While these quantities are all negative, they are much less so than when the TF_4 is allowed to freely adjust its internal geometry to the incoming base. The energetic cost to this restriction is listed in the next column of Table 7. While fairly small for the weakly bound complexes in the first two rows, it is quite substantial, above 20 kcal/mol, for many of the others. So in principle, it would be possible for a base to form a tetrel-bonded attachment within the acid, even if the latter were unable to alter its internal geometry to better accommodate the base. But such a TB would be very much weakened by this rigidity.

With regard to the electrostatic attraction that draws in the base, it is typical to consider this concept within the context of the depth of the σ-hole, which is in turn usually assessed as the magnitude of the maximum of the MEP on the 0.001 au isodensity surface of the optimized acid monomer, V_{max}. But this protocol neglects the geometric deformations that occur with the acid as the base approaches, which can be quite substantial, in particular for a tetrel-acid. The opening of the TF_4 umbrella causes very large enhancements in V_{max}, which are obvious in the last two columns of Table 7. As an example, the flattening of the SiF_4 pyramid upon approach of the NH_3 base more than doubles the σ-hole depth.

In summary, the deepening of the σ-hole that arises as the TF_4 acid is deformed to accommodate the approach of the base enhances the electrostatic attraction, and mitigates the energetic cost of this internal deformation.

Another manifestation of the implications of deformation arises in connection with a system wherein the T is covalently attached to three F atoms and a substituted phenyl ring [37]. The σ-hole lying opposite any of the F atoms is deeper than that opposite the ring within the tetrahedral molecule. However, the incorporation of a NH_3 base via a TB requires the distortion into a trigonal bipyramid shape. This transition reverses the depths of these two σ-holes, leading in turn to a higher interaction energy when the base lies opposite the ring. On the other hand, the deformation required to incorporate the base in this position is larger than when the base lies opposite a F atom. The final result is a fine balance between these two effects, so the preferred conformation depends on the size of the central T atom.

CARBON AS TETREL BOND PARTICIPANT

As described above the ability to participate in a noncovalent bond of the sort described here requires the bridging atom to be able to develop a positively charged σ-hole region. This ability depends in large part on electropositivity, coupled with a polarizable electron cloud. Both of these properties diminish as one moves up a column of the periodic table. It is for this reason that F is seldom involved as electron acceptor in halogen bonds, and the same is true of the other first-row atoms O and N within the context of chalcogen and pnicogen bonds, respectively [38]. One would therefore anticipate that C would be a reluctant participant in tetrel bonds. On the other hand, the overwhelming importance of this atom in chemistry and biology makes this issue

one of over-riding importance. A great deal of recent effort has therefore been devoted to the question as to whether C can participate in tetrel bonds, and if so, under what conditions.

The importance of tetrel bonds in biology, particularly those involving C, was emphasized by a survey of protein structures [39] which placed emphasis on the CF_3 parallel of the methyl group. The authors stressed the importance of these bonds in such systems as the $NADP^+$-dependent isocitrate dehydrogenase (IDH) enzyme and its interaction with an aspartate residue, as well as a triazine-based inhibitor of enasidenib. Calculations showed strong TBs between the CF_3 group and a variety of bases. Later surveys extended these TBs to the unsubstituted methyl group. One study for example [40] noted 8358 such interactions, that were present in a variety of different secondary protein structures.

With respect to the methyl group, due to its importance, the ability of methyl groups to participate in TBs has engendered a good deal of study [41, 42]. Such a bond is possible when the Me is situated on an aromatic ring as in TNT [43]. In a broader sense, the tetrel bonding of the methyl group has been substantiated by crystal structure surveys of various types. The criteria invoked involve distance and angles. The typical criteria require first that the R(C--X) distance be less than the sum of vdW radii of the two atoms. The angular aspect places a minimum on the θ(R-C··X) angle of perhaps 120°, applying the concept that this angle tends toward linearity. Mooibroek [44] examined both the CSD and PDB and found strong directional statistical evidence of tetrel-bonding methyl groups. 164 TBs were observed in a survey of CSD crystal structures when a methyl group is approached by a halide [9]. The participation of methyl groups in such bonds appears to be more general than that, covering a range of different bases as well as substitutions on the methyl group [45].

Another such study focused on a particular class of enzymes that facilitate transfer of methyl groups, the S-adenosylmethionine-dependent methyltransferases [46]. The criteria were fairly stringent, requiring an angle of at least 160°. Nevertheless, this survey identified a number of relevant arrangements of a methyl group, most employing O as electron donor atom. Some of the partner molecules were other components of the enzyme itself, while others were solvent molecules. Quantum calculations were applied to a number of these systems where energetics and other aspects of the wave functions qualified these interactions as true tetrel bonds.

Computational Examination

The specific ability of C within a methyl group to engage in TBs was verified by Varadwaj et al [47] when they paired a number of CH_3R molecules with both ends of CO. The interactions were rather weak, well under 1 kcal/mol, but their presence was verified by AIM, NCI, and NBO analyses, as well as the presence of small shifts in the C≡O vibrational frequency. Curiously, the direction of this shift, to the red or blue, depended upon whether it was the C or O atom of CO which was interacting with the methyl group. The P atom appears capable of serving as the nucleophilic center in TBs as well [48], and the σ-bond of H_2 may do so as well [49].

The ability of a methyl group to participate in a TB was assessed in both a neutral and cationic setting [50], where its strength could be directly compared to both H-bonds and chalcogen

bonds. N-methylacetamide (NMA) was taken as the common base through its amide O atom. Fig 5 depicts a number of ways in which this base can bind to the $FHSMe^+$ cation. Fig 5a illustrates a TB wherein the NMA O atom lies along the extension of the S··C bond axis, where the O is separated from the C by some 2.591 Å. Figs 5b and 5c illustrate HBs, with the CH in b and the SH in c. Another mode of interaction concerns the S atom, via a chalcogen bond (YB), either opposite the F in Fig 5d or the CH_3 in 5e.

The first row of Table 8 shows [50] that the strongest binding involves the latter FS··O YB at 39 kcal/mol. The SH··O HB is a bit weaker at 34 kcal/mol, followed by the other YB, CS··O, at 23 kcal/mol. The CH··O HB is still weaker at 21, followed finally by the tetrel bond at 17 kcal/mol. Two other cationic Lewis acids considered here removed the F atom, yielding $CH_3SH_2^+$ and $(CH_3)_3S^+$. The SH··O HB retains its position as the strongest interaction for the former where it is possible. When the S is surrounded by three methyl groups the YB and HB remain preferred over the TB, although the latter remains fairly strong at 13.7 kcal/mol. Removing the positive charge from the Lewis acid weakens all interactions, but not uniformly, as is evident in the last two rows of Table 8. Nonetheless, any possible FS··O YB remains the preferred binding option, followed by a CH··O HB. A SH group is a strong electron acceptor, making the SH··O HB the most stable configuration for MeSH. Summarizing the standing of the Me TB, it is usually the weakest interaction of those available, when compared to HB or YB arrangements. Nevertheless, its binding energy is not negligible, on the order of 2 kcal/mol for neutral acids, and rising to the 14-17 kcal/mol range when the acid is a cation.

The placement of a base directly along the R-C bond extension of a $R\text{-}CH_3$ methyl group is of course consistent with a tetrel bond. On the other hand, prior observations of this sort of arrangement had generally been attributed to a trifurcated HB, i.e. one in which the base interacts not directly with the central C, but rather with the three H atoms. This contention raises the question as to how one might distinguish between the two: what specific markers might be present. Bauzá and Frontera addressed this question [51] by placing a nucleophile along the R-C extension and then determining its final optimized position. The AIM bond path led from the nucleophile to the central C atom unless the nucleophile was moved from its central location at which point the bond path would switch to a methyl H atom. A search of PDB crystal structures led to a preponderance of central locations for the nucleophile. From a theoretical perspective an analysis of the wave function by NBO or AIM or a related method might provide some clues as to how to best characterize the interaction. But if one observes a structure of this sort in an experimental context, how might the distinction be made? Since the structural features are the same for either interpretation, a spectroscopic analysis might provide some key information.

This issue was investigated [52] through a quantum chemical study that simultaneously offered both wave function and spectroscopic data for purposes of comparison. Several different systems were devised, each of which contained a putative nonbonding interaction between a methyl group and a base. Several of these systems are pictured in Fig 6 which defines the pertinent geometrical parameters. R refers to the distance between the methyl C and the electron donor atom of the base. Most important here is θ(RC··N/O) which is equal to 180° when the

nucleophile is situated directly along the R-C bond extension. This angle diminishes to roughly 110° when the base atom is aligned along a C-H bond, making the interaction clearly of the HB variety. Systems were chosen to cover a wide range of types, including neutral-neutral, cation-neutral, cation-anion, neutral-anion, and considering both O and N as electron donor atoms.

The effects of either a HB or TB upon the vibrational and NMR spectra of $SMe_3^+\cdot\cdot NH_3$ are illustrated in Fig 7a and 7b, respectively [52]. The left side of the figure corresponds to a θ angle of 180° designated as a TB, while the HB is represented by the right side with θ=110° for which the N atom aligns directly along the CH axis. The plotted data refer to the changes in each quantity relative to the uncomplexed monomer. The solid curves in Fig 7a correspond to the stretching vibrational frequencies of the methyl groups, while the bending motions are denoted by broken curves. In each case, the red and blue curves refer to symmetric and asymmetric modes respectively. With respect first to the stretching motions, formation of a TB produces a small blue shift, but as the base swings around toward a HB, these frequencies drop, particularly the symmetric stretch. The bending modes behave in the opposite manner. The TB causes a substantial red shift, which shifts to the blue as the base swings around to a H-bonding position.

Fig 7b displays the changes in NMR chemical shielding within the methyl group upon formation of the complex. The orange curve refers to the H atom which engages via a HB, whereas the green curve indicates the average of all three methyl protons, since these 3 signals are difficult to distinguish during an NMR experiment. The blue curve shows that the methyl C atom undergoes a large deshielding in the TB, which rapidly diminishes in magnitude as the system transits to a HB. The H atoms behave in the opposite manner, with a small deshielding in the TB configuration growing larger for the HB, particularly for the bridging proton itself.

While there are some quantitative differences for the six systems examined, they all obey similar trends as exhibited in Fig 7, that ought to serve as useful signposts as to the type of bond present based upon spectral observations [52]. The methyl CH stretches are blue-shifted in a TB, while a HB shifts them to the red; the opposite pattern characterizes the bending modes. The methyl C atom suffers a good deal of deshielding within the TB configuration which is reduced, or even reversed, in the HB. The methyl H atoms are deshielded to a much higher degree within a HB as compared to a TB.

Source of NMR Shifts

The forgoing NMR data raises an interesting question concerning the source of the deshielding that occurs upon formation of a TB or HB for that matter. As elaborated earlier, the formation of either of these noncovalent bonds will cause certain geometric deformations within the monomer, which in turn affect the MEP surrounding each subunit, with implications for the binding energetics. But these same structural changes can be supposed to also affect the NMR shielding around the various nuclei. This point raises the interesting question as to whether the shielding changes occurring on the various nuclei are a direct result of the electronic perturbations caused by the noncovalent bond formation, or less directly due to the changes that the bonding induces within the internal geometries of the subunits.

This question was addressed [53] within the context of the four Lewis acids considered above, SEt_2Me^+, NMe_4^+, SMe_2, NMe_3, all of which displayed shielding changes on the C and H atoms of their methyl groups. The CH bonds of these monomers were stretched, but in the absence of a base, so as to extract the effect of this geometric change in and of itself. The C shielding diminished by roughly 2 ppm for a r(CH) stretch of 0.01 Å, while that of H dropped by only 0.3 ppm. The deshieldings caused purely by the bond length changes are far too small to account for the amounts that are computed when the nucleophile is actually present, which leaves the electronic perturbations as the primary factor.

C as Electron Donor

The same high electronegativity that inhibits the ability of C to serve as electron acceptor ought to work in the opposite direction, facilitating its functioning as a donor. Of course, the absence of a lone pair on C in its typical tetravalent bonding eliminates the possibility of donation from this particular orbital. However, there are other, admittedly uncommon, bonding scenarios where C does contain a lone pair which might act to donate electrons [54]. Li et al [55] extended the idea of TB to encompass an open-shell methyl radical as a potential electron donor in a series of $FTH_3\cdots CH_3$ complexes, and went on to explore issues of cooperativity. A CH_3 radical donor was later studied by Esrafili [56] who identified a bit of back-bonding to amplify the interaction. Carbenes serve as an alternate type of electron donor [29, 57-62], engaging for example [63] in C··C TBs with CO_2, or bonds [59] between CH_3R and CH_2. A more recent example of a bonding type with such possibilities is drawn from the carbone family [64-67] where the divalent C atom is endowed with two lone pairs. Imparting a full negative charge to the C-containing entity also permits interactions through a C lone pair, e.g CN^- [68-72], or an alkyl anion such as $CH_3CH_2^-$ [73].

Another type of scenario avoids the necessity of a lone pair on C entirely. If a highly electron-releasing substituent such as a metal atom M, is added to C, the latter acquires a strong enough partial negative charge that it can attract a Lewis acid. The minimum in the MEP arising from the excess density leads to what may be termed a "σ-lump" along the extension of the C-M bond axis, in analogy with the σ-hole that signifies an electron deficiency. A CH_3M group can thus engage in a "ditetrel" bond with a FTH_3 Lewis acid, donating charge not from a C lone pair, but rather through its σ(CM) bonding orbital [74]. This phenomenon brings to full circle the analogies between HBs and TBs, as this ditetrel bond is a close parallel to the better known dihydrogen bond. This idea of a TB between two T atoms has been noted in the framework of a pair of Sn atoms [75] in various crystals, whose characterization as a noncovalent bond was verified by quantum calculations. It is not only a CH_3M monomer which can use σ-orbitals as electron donor, but also the hydride segment of MH bonds [76] when allowed to interact with TH_3F.

SPECTROSCOPY

The forgoing has highlighted the light that spectroscopy, and in particular IR and NMR, can shine on our understanding of the fundamentals of hydrogen and tetrel bonding. These same ideas can be applied to the other closely related noncovalent bonds. Table 9 presents spectroscopic and energetic information [77] concerning HB and TB complexes, as well as halogen, chalcogen, and pnicogen bonds. The common base in all cases is the O atom of N-methylacetamide (NMA) chosen by virtue of its similarity to the peptide bond within proteins. The H-bonding systems cover the full range of HX acids, with X representing a halogen. The other Lewis acids all place a F atom on a X, Y, Z, or T atom so as to form the requisite σ-hole, with the latter atoms chosen from the second, third, and fourth rows of the periodic table.

The energetics in the first column of Table 9 [77] indicate that all bonds strengthen as the bridging atom grows larger, e.g. Si < Ge < Sn (with the exception of HBs for which a proton acts as bridge in all cases). Regarding different sorts of bonds, it would appear that halogen bonds are strongest, followed by chalcogen, and then by pnicogen and tetrel: XB > YB > ZB ~ TB. The next column indicates a red shift of all ν(FA) stretching frequencies. These shifts adhere to the energetic ordering of the different sorts of bonds, but unlike the energetics the shifts become smaller as the central A atom grows larger. This latter trend is likely due A's heavier mass which lowers its vibrational frequency. The red shifts are all consistent with the bond weakening that results from charge transfer into the σ*(FA) antibonding orbital. The formation of the noncovalent bond exerts an effect upon the electron donor molecule as well, as measured by the red shift in the C=O stretching frequency of NMA. While smaller in magnitude than Δν(FA), the red shift of the C=O stretch is substantive, certainly large enough to be measured, so is of some practical significance. These shifts are also roughly proportional to the bond energetics.

The last five columns of Table 9 display the changes in chemical shielding of atoms on both the Lewis acid and base entities [77]. Although the central proton is deshielded within the HBs, one sees the opposite effect of a shielding increase on the larger central A atoms, and quite a substantial one. The F atom lying opposite the base suffers a drop in its shielding. With regard to the base, the O atom directly involved in the noncovalent bond sees an increase in its shielding, and one which is again roughly proportional to the bond strength. Both the C and N atoms are deshielded by amounts on the order of 4-8 ppm. So there is a consistent pattern to the NMR spectra that might be used as a fingerprint in order to detect these bonds within an experimental situation. It might be added that a parallel study [78] switched out the base to the smaller NH_3, and encountered similar trends. The only difference was that the stronger noncovalent bonds formed with NH_3 resulted in somewhat larger frequency and shielding changes. Although a recent work [79] did not explicitly include tetrel bonds, a fairly tight connection was found between these spectroscopic markers and noncovalent bond strength of a long list of diverse acid-base pairs that involved pnicogen, chalcogen, and halogen atoms, so one would expect the same to be true for TBs as well.

There have been spectroscopic measurements pertaining to tetrel bond strength [80], particularly through solid state ^{13}C NMR. The C=O and C≡N groups have been considered as

electron donors, complemented by acceptor groups NC, SC, and their cationic equivalents. Among some of the chief findings is the sensitivity of chemical shielding to the intermolecular distance, as opposed to the interaction energy. For example, the shift of ^{13}C drops as the intermolecular distance shortens. Recent NMR data have shown that tetrel bonds, in particular Sn··Cl interactions observed in the crystal can persist when transferred to solution [81]

DIRECT COMPARISON OF TETREL WITH OTHER NONCOVALENT BONDS

Given the diversity within σ-hole interactions, but also the similarities in terms of the roots of their binding, it is logical to wonder if there is some hierarchy amongst them in terms of which bonds are the strongest, and which weakest. There have been some attempts in this regard. When substituted methanes are paired with halide electron donors [82], one study found TBs to be intermediate between HBs and XBs. A comparison was drawn between tetrel and pnicogen bonds when both $FGeH_3$ and $FAsH_2$ were paired with a common base [83].

A unified means of addressing this question starts with an unsubstituted AH_n molecule, where A is drawn from the X, Y, Z, and T families, but is taken from the third row of the periodic table in each case for purposes of uniformity. Table 10 presents this comparison [84] where Lewis acids are combined with NH_3 as universal base. The uppermost segment of Table 10 relates to the fully hydrogenated acids HBr, H_2Se, H_3As, and H_4Ge, as a baseline for unsubstituted systems. Without an electron-withdrawing substituent, these bonds are fairly weak, and follow the order YB > XB >ZB > TB with the TB the weakest. The binding decreases when a single Me group is added to the acid, due to the electron-releasing power of this alkyl substituent. With this addition, the YB remains the strongest, followed now by the ZB, with XB and TB taking up the rear. The next segment of Table 10 retains one H but fills up the remaining substituent shell with F atoms, one for Se, two for As, and three for Ge. It is now the TB which is the strongest of the subgroup, which may be associated with the number of electron-withdrawing F atoms. The lowermost section of Table 10 replaces the H of the previous group by Me. Again, the electron-releasing alkyl weakens all the bonds, but retains the order TB > ZB > YB.

Inspection of the intermolecular distances in the next column of Table 10 reveals a similar story. These lengths generally shorten as the noncovalent bond strengthens. The orientation angles in the last column show that the TBs are quite linear, with θ(RGe··N) consistently equal to 180. The presence of lone pairs on the other central atoms tends to shift the σ-hole off of the R-A bond extension, and accounts for the angles less than 180° in those cases. In summary, a TB will outpace the other bonds in the sense that it can accommodate a larger number of electron-releasing groups. But in the absence of any such substituents, the TB is slightly weaker than its counterparts.

An alternate means of comparing noncovalent bond strengths places the two atoms of interest on the same molecule in direct competition for a base. Consider the $GeBrF_3$ molecule, for example. Just as a σ-hole will be present on the Br atom on the extension of the Ge-Br bond, a similar such hole ought to open on the Ge atom. In principle, a base could interact with either of

these two holes, leading to a halogen or tetrel bond, respectively. Examples of these two types of bonds [85] are presented in Fig 8a and 8b for the common base NH_3. These diagrams also show that the XB is considerably longer than the TB, by a full Å.

And indeed the TB is stronger than the XB, not just for the specific case of GeF_3Br, but also for most of the general TF_3X molecules. As may be seen by the first two columns of data in Table 11, the interaction energies of the TBs are in the 35-38 kcal/mol range, as compared to the considerably weaker XB binding energies of less than 6 kcal/mol [85]. Note that these findings remain in force regardless of the nature of either the T or X atoms. The prime exception to these patterns concerns the C atom in the first few rows of the Table. The higher electronegativity of C than its T counterparts weakens the TB to less than 2 kcal/mol, while raising the XB energies to the 3-7 kcal/mol range. The intermolecular distances are consistent with these notions. In most cases, the TB distance is very much shorter than R(X··N), with T=C providing the main exceptions. So when placed in the same covalent bond, the tetrel atom offers a much stronger interaction with a base than does a halogen.

One might be tempted to attribute this contrast to the three electron-withdrawing F substituents attached directly to the T atom in TF_3X. However, this pattern is little altered when the F atoms are all changed to H [85]. Of course, the removal of the F atoms weakens the σ-hole on the T and X atoms, which in turn reduces the interaction energies. And it is also true that this F removal affects the TB more than it does the XB. But what remains in force is the fact that the TBs are both stronger and shorter than the XBs (again with the exception of T=C).

OTHER ASPECTS OF TETREL BONDS

Given the fact that a tetravalent TR_4 molecule contains four σ-holes, there is some reason to wonder whether a given T atom might be able to accommodate more than one TB. Indeed, TF_4 can involve itself in two simultaneous TBs [86] to a pair of NCH bases. In order to do so, the entire hexacoordinated system distorts into an octahedral shape. There is an interesting energetic competition between the cis and trans positioning of the two bases. Whereas the latter affords a more favorable interaction energy, its high deformation energy makes it less energetically accessible than is the cis structure.

The concept of a σ-hole, which is associated with a tetrel bond is not limited to tetravalent TR_4 molecules. Many tetrel atoms, particularly the heavier ones, commonly engage in higher orders of bonding, which might be considered hypervalent. Gnanasekar and Arunan [87] considered this issue as to the underlying nature of the bonding within the TH_5^+ cation. They concluded that whereas CH_5^+ contains five C-H bonds around a hypervalent C, both SiH_5^+ and GeH_5^+ are better described as a neutral H_2 molecule which is tetrel bonded to a TH_3^+ ion. Pb in particular engages in such bonding patterns [88-90] while still being able to engage in a TB. One such study [91] went so far as to evaluate the tetrel-bonding capability of Pb when surrounded by eight ligands. With regard to hypervalent structures, there have emerged a number of reviews of tetrel, as well as other sorts of noncovalent bonding [92-95]. In a broader context, halogen,

chalcogen, and pnicogen bonds can also involve hypervalent central atoms [96], pnicogen bonds being particularly strong.

Whereas the σ-hole that lies directly along the extension of a T-R covalent bond is a common means of constructing a TB, there are alternatives. The planar arrangement around T when in its sp^2 hybridization leads to important modifications. There are no longer any positive regions that lie directly opposite any of the T-R bonds, all of which lie in a common plane. On the other hand, the MEP surrounding the system typically contains positive regions that lie above and below this plane. These so-called π-holes are fundamentally different than the σ-holes in terms of their root cause, which derive from a smaller density above the molecular plane than within it. There is also a difference in terms of the charge transfers, which shift density into the π* orbitals, which are typically as closely associated with the R substituent as with the T atom itself.

Tang and Li [97] verified the viability of a π type of TB when they placed a H-bonded NCH··NCH dimer above the $F_2T{=}O$ plane for the two lightest T atoms C and Si, which also displayed elements of cooperativity. Another study [98] replaced O by its heavier Se and Te congeners and also considered the cooperative effects of a pair of NCH molecules, engaging in both tetrel and chalcogen bonds with the central $F_2T{=}Y$. This same sort of planar unit was considered as electron acceptor [99] from IF with interaction energies of nearly 10 kcal/mol. Shen et al took another look at the π-hole of F_2TO, this time pairing it with various unsaturated hydrocarbons [100] acetylene, ethylene, 1,3-butadiene and benzene as π-donors, which amounted to π-π interactions. Nonetheless, the systems obeyed the usual rules of heavier T atoms associated with stronger bonds.

Xu et al [101] carried out a direct comparison of σ with π-hole TBs, using TH_3F and F_2TO as the corresponding acids, and found the π-hole bonds to be the stronger of the two, when combined with the N atoms of pyrazine and 1,4-dicyanobenzene. These authors also delved into cooperativity effects. Wei and Li [102] made a similar σ vs π comparison using cyanoacetaldhyde as the base, although the comparison was clouded by secondary interactions. Yet another take on this competition between σ and π-holes arose in calculations [103] where both TH_3F and F_2TO interacted with a similarly planar H_2CY, where Y=O,S,Se. Both the σ- and the π-hole interactions are weakened by heavier chalcogen atoms, while the π-hole interaction involving F_2TO (T=Ge, Sn, and Pb) changes in the opposite direction. One interesting issue derived here is that F_2SiO and H_2CX go beyond a noncovalent tetrel bond and combine to a single unit.

A specific comparison of π-hole TBs with their σ-counterparts [104] found the former bonds with NH_3 to be stronger than the latter, even though the depths of the π/σ holes were comparable. A similar comparison emerged when the base was altered to borazine [105] which involved approach of the T from above the plane of the borazine. Wei et al showed how the presence of a π tetrel bond can exert an influence on a neighboring H-bond, even to the extent of promoting a proton transfer [106].

The sp hybridization, as in O=C=O can also furnish a π-hole above the C atom. This positive region has been exploited in bonding to glycine [107] and to azines [108]. In the latter case, it was found that increasing the number of N atoms in the aromatic ring leads to a gradual weakening of

the TB. Incorporating a number of OCO molecules into a cluster [109] allows multiple TBs to participate in the total binding, along with chalcogen and CH··O H-bonds. Replacement of one O by S, allows the O=C=S variant [110] to engage in not only tetrel bonds but also chalcogen bonds. Other replacements to ONN and SCS [111] have allowed comparisons of the TBs to pnicogen and chalcogen bonds within the sp-hybridized framework. The latter work demonstrated a strong correlation between the dissociation energy of each complex and the intermolecular force constant. When paired with HN(CH)SX azine, OCS [112] engages in a C··N tetrel bond, accompanied by a S··O chalcogen bond. π-holes wherein C is bound to another atom can also be involved in TBs, as in XC≡N molecules [113]. The same sp-hybridization allows the two C atoms of an alkyne like RC≡CR to engage in a TB to another C atom in a sp^3 TH_3F unit, with an interesting inter-C TB. Tetrel bonds between C atoms were also examined [57] in the context of N-heterocyclic carbenes serving as electron donor to CO_2. When CO_2 is associated with various azoles [114], the strength of the TB diminishes as the number of N atoms in the ring rises. Pairs of π-holes can engage in TBs, as for example in the combination of CO_2 with $X_2T=O$ [115].

Just as in the case of H-bonds, one would expect that the presence of two TBs where the central unit acts simultaneously as both electron donor and acceptor, ought to strengthen both bonds in what is commonly referred to as positive cooperativity or synergy. And numerous studies have confirmed this idea. McDowell introduced the ideas of cooperativity to the TB field [116] in that a CH_3^- anion could interact favorably with a pair of XF molecules, via a pair of TBs. Note that the ability of C to engage in TBs, especially two simultaneously, is aided by its anionic charge. This same author later considered [117] cooperativity between TBs and halogen, hydrogen, and pnicogen bonds. The Esrafili group has been particularly active in studies of cooperativity of tetrel bonds [118-120], considering $(CH_3CN)_n$ and $(CH_3NC)_n$ [121]. Other types of arrangements include linear chains of H_3SiCN and H_3SiNC [122] or a set of NC-TR_3 units [123]. Cooperativity with triel bonds was considered [124], as were HBs [125] and pnicogen bonds [126]. Wang et al [127] pursued the question of cooperativity between π-hole TBs and halogen bonds. Noncovalent bonds involving π-holes are no exception to this idea, as for example with halogen bonds [128]. One manifestation of this cooperativity emerges in the context of the proton affinity of silanol and siloxane when their Si atoms are engaged in a TB [129].

In an interesting twist, the level of cooperativity can affect the competition between two different sorts of bonds. TF_3OH is capable of forming a OH··N H-bond with an N-base, as well as a T··N TB. It is the former which is preferred for most T atom [130]. However, if $MgCl_2$ is added to the system it will engage in a Mg··O interaction with TF_3OH. This latter Mg-bond enhances both the HB and TB, but by different amounts. While the HB enhancement is slightly diminished as T grows larger, the TB behaves in the opposite manner.

It probably goes without saying that the presence of a full positive charge on the Lewis acid, or a negative charge on the base, will amplify the strength of any interaction, the TB being no exception. Among numerous illustrations in the literature on this topic, one might mention several recent studies [8, 131-133]. There are practical aspects to this property. For example, various

anions can be selectively bound by bipodal receptors via tetrel and related noncovalent bonds [134-137].

Just as in the case of hydrogen and other related noncovalent bonds, TBs are not limited to fully separate units, sometimes occurring in an intramolecular context. As one example, Marín-Luna et al [138] considered such bonds within atranes. Another work [139] focused on C=N⋯C-X sort of intramolecular TB involving charge transfer from the N lone pair to the σ*(CX) antibonding orbital. Indeed, it is logical to surmise that intramolecular tetrel bonds will be a common occurrence, as is the case for H-bonds.

A good deal of the original data described in this work involved the use of the polarized correlation-consistent double-ζ aug-cc-pVDZ basis set. This set has established itself as a workhorse in many calculations of noncovalent bonds, and yields generally accurate results [140-156]. When used in tandem with an MP2 treatment of electron correlation, this set provided binding energies [157] with errors of less than 0.5 kcal/mol, and another work [158] found very good accuracy in comparison with CCSD(T)/CBS, or provided an excellent reproduction of anisotropy [159]. Extension to an analogous triple-ζ aug-cc-pVTZ set and even quadruple-ζ, and the complete basis set limit does not change the results by very much [8, 34, 85, 105, 109, 113] in the specific context of tetrel bonds.

Acknowledgements
This material is based upon work supported by the National Science Foundation under Grant No. 1954310.

Conflict of interest
The author has no conflicts of interest to declare.

REFERENCES

1. D. Mani and E. Arunan, *Phys. Chem. Chem. Phys.*, 2013, **15**, 14377-14383.
2. A. Bauzá, T. J. Mooibroek and A. Frontera, *Angew. Chem. Int. Ed.*, 2013, **52**, 12317-12321.
3. A. Bauza, T. J. Mooibroek and A. Frontera, *Chem. Commun.*, 2014, **50**, 12626-12629.
4. D. Mani and E. Arunan, *J. Phys. Chem. A*, 2014, **118**, 10081-10089.
5. K. J. Donald and M. Tawfik, *J. Phys. Chem. A*, 2013, **117**, 14176-14183.
6. M. Liu, Q. Li, J. Cheng, W. Li and H.-B. Li, *J. Chem. Phys.*, 2016, **145**, 224310.
7. S. J. Grabowski, *Applied Organometallic Chemistry*, 2017, **31**, e3727.
8. M. Liu, Q. Li and S. Scheiner, *Phys. Chem. Chem. Phys.*, 2017, **19**, 5550-5559.
9. E. Bartashevich, Y. Matveychuk and V. Tsirelson, *Molecules*, 2019, **24**, 1083.
10. S. J. Grabowski, *Phys. Chem. Chem. Phys.*, 2014, **16**, 1824-1834.
11. Y. Kawashima, R. D. Suenram and E. Hirota, *J. Chem. Phys.*, 2016, **145**, 114307.
12. C. Calabrese, W. Li, G. Prampolini, L. Evangelisti, I. Uriarte, I. Cacelli, S. Melandri and E. J. Cocinero, *Angew. Chem. Int. Ed.*, 2019, **58**, 8437-8442.
13. S. Gao, D. A. Obenchain, J. Lei, G. Feng, S. Herbers, Q. Gou and J.-U. Grabow, *Phys. Chem. Chem. Phys.*, 2019, **21**, 7016-7020.
14. T. Lu, J. Zhang, Q. Gou and G. Feng, *Phys. Chem. Chem. Phys.*, 2020, **22**, 8467-8475.
15. M. Li, J. Lei, G. Feng, J.-U. Grabow and Q. Gou, *Spectrochimica Acta Part A: Molecular and Biomolecular Spectroscopy*, 2020, **238**, 118424.
16. A. Franconetti and A. Frontera, *Chem. Eur. J.*, 2019, **25**, 6007-6013.
17. G. Mahmoudi, M. Abedi, S. E. Lawrence, E. Zangrando, M. G. Babashkina, A. Klein, A. Frontera and D. A. Safin, *Molecules*, 2020, **25**, 4056.
18. F. Akbari Afkhami, G. Mahmoudi, F. Qu, A. Gupta, E. Zangrando, A. Frontera and D. A. Safin, *Inorg. Chim. Acta*, 2020, **502**, 119350.
19. E. D. Stevens, *Mol. Phys.*, 1979, **37**, 27-45.
20. S. C. Nyburg and W. Wong-Ng, *Proc. R. Soc. Lond. A*, 1979, **367**, 29-45.
21. S. Ikuta, *J. Mol. Struct. (Theochem)*, 1990, **205**, 191-201.
22. J. P. M. Lommerse, A. J. Stone, R. Taylor and F. H. Allen, *J. Am. Chem. Soc.*, 1996, **118**, 3108-3116.
23. S. J. Grabowski and E. Bilewicz, *Chem. Phys. Lett.*, 2006, **427**, 51-55.
24. V. R. Hathwar and T. N. G. Row, *J. Phys. Chem. A*, 2010, **114**, 13434-13441.
25. R. Sedlak, M. H. Kolář and P. Hobza, *J. Chem. Theory Comput.*, 2015, **11**, 4727-4732.
26. F. A. Bulat, A. Toro-Labbé, T. Brinck, J. S. Murray and P. Politzer, *J. Mol. Model.*, 2010, **16**, 1679-1691.
27. S. Scheiner, *J. Phys. Chem. A*, 2017, **121**, 5561-5568.
28. C. Wang, Y. Aman, X. Ji and Y. Mo, *Phys. Chem. Chem. Phys.*, 2019, **21**, 11776-11784.
29. H. Lin, L. Meng, X. Li, Y. Zeng and X. Zhang, *New J. Chem.*, 2019, **43**, 15596-15604.
30. S. A. C. McDowell, R. Wang and Q. Li, *Molecules*, 2020, **25**, 4197.
31. M. Marín-Luna, I. Alkorta and J. Elguero, *Theor. Chem. Acc.*, 2017, **136**, 41-48.
32. S. J. Grabowski and W. A. Sokalski, *ChemPhysChem.*, 2017, **18**, 1569-1577.
33. A. C. Tagne Kuate, M. M. Naseer, M. Lutter and K. Jurkschat, *Chem. Commun.*, 2018, **54**, 739-742.
34. S. Scheiner, *J. Phys. Chem. A*, 2018, **122**, 2550-2562.
35. W. Zierkiewicz, M. Michalczyk, R. Wysokiński and S. Scheiner, *Molecules*, 2019, **24**, 376.

36. W. Zierkiewicz, M. Michalczyk and S. Scheiner, *Phys. Chem. Chem. Phys.*, 2018, **20**, 8832-8841.
37. R. Wysokiński, M. Michalczyk, W. Zierkiewicz and S. Scheiner, *Phys. Chem. Chem. Phys.*, 2019, **21**, 10336-10346.
38. Z. Latajka and S. Scheiner, *J. Chem. Phys.*, 1986, **84**, 341-347.
39. X. García-Llinás, A. Bauzá, S. K. Seth and A. Frontera, *J. Phys. Chem. A*, 2017, **121**, 5371-5376.
40. V. R. Mundlapati, D. K. Sahoo, S. Bhaumik, S. Jena, A. Chandrakar and H. S. Biswal, *Angew. Chem. Int. Ed.*, 2018, **57**, 16496-16500.
41. M. M. Szczesniak, G. Chalasinski, S. M. Cybulski and S. Scheiner, *J. Chem. Phys.*, 1990, **93**, 4243-4253.
42. Z. Latajka and S. Scheiner, *J. Comput. Chem.*, 1987, **5**, 674-682.
43. M.-Z. Ao, Z.-q. Tao, H.-X. Liu, D.-Y. Wu and X. Wang, *Comput. Theor. Chem.*, 2015, **1064**, 25-34.
44. T. J. Mooibroek, *Molecules*, 2019, **24**, 3370.
45. A. Daolio, P. Scilabra, G. Terraneo and G. Resnati, *Coord. Chem. Rev.*, 2020, **413**, 213265.
46. R. C. Trievel and S. Scheiner, *Molecules*, 2018, **23**, 2965-2981.
47. P. R. Varadwaj, A. Varadwaj and B.-Y. Jin, *Phys. Chem. Chem. Phys.*, 2014, **16**, 17238-17252.
48. A. Slassi, S. M. Gali, A. Pershin, A. Gali, J. Cornil and D. Beljonne, *J. Phys. Chem. Lett.*, 2020, **11**, 4503-4510.
49. S. J. Grabowski, *Molecules*, 2020, **25**, 3294.
50. S. Scheiner, *J. Phys. Chem. A*, 2015, **119**, 9189-9199.
51. A. Bauzá and A. Frontera, *Cryst.*, 2016, **6**, 26.
52. S. Scheiner, *J. Phys. Chem. A*, 2018, **122**, 7852-7862.
53. S. Scheiner, *Chem. Phys. Lett.*, 2019, **714**, 61-64.
54. S. Scheiner, *Polyhedron*, 2021, **193**, 114905.
55. Q. Li, X. Guo, X. Yang, W. Li, J. Cheng and H.-B. Li, *Phys. Chem. Chem. Phys.*, 2014, **16**, 11617-11625.
56. M. D. Esrafili and F. Mohammadian-Sabet, *Struct. Chem.*, 2016, **27**, 1157-1164.
57. J. E. Del Bene, I. Alkorta and J. Elguero, *J. Phys. Chem. A*, 2017, **121**, 8136-8146.
58. J. E. Del Bene, I. Alkorta and J. Elguero, *ChemPhysChem.*, 2017, **18**, 1597-1610.
59. M. Liu, Q. Li, W. Li and J. Cheng, *Struct. Chem.*, 2017, **28**, 823-831.
60. M. D. Esrafili, F. Mohammadian-Sabet and E. Vessally, *Mol. Phys.*, 2016, **114**, 2115-2122.
61. D. Pathak, S. Deuri and P. Phukan, *J. Phys. Chem. A*, 2016, **120**, 128-138.
62. I. Alkorta, F. Blanco, J. Elguero, J. A. Dobado, S. M. Ferrer and I. Vidal, *J. Phys. Chem. A*, 2009, **113**, 8387-8393.
63. J. E. Del Bene, I. Alkorta and J. Elguero, *J. Phys. Chem. A*, 2017, **121**, 4039-4047.
64. C. Esterhuysen and G. Frenking, *Chem. Eur. J.*, 2011, **17**, 9944-9956.
65. J. E. Del Bene, I. Alkorta and J. Elguero, *Phys. Chem. Chem. Phys.*, 2020, **22**, 15966-15975.
66. R. Tonner and G. Frenking, *Chem. Eur. J.*, 2008, **14**, 3273-3289.
67. R. Tonner, F. Öxler, B. Neumüller, W. Petz and G. Frenking, *Angew. Chem. Int. Ed.*, 2006, **45**, 8038-8042.

68. W. Zierkiewicz, R. Wysokiński, M. Michalczyk and S. Scheiner, *ChemPhysChem.*, 2020, **21**, 870-877.
69. R. Wysokiński, W. Zierkiewicz, M. Michalczyk and S. Scheiner, *ChemPhysChem.*, 2020, **21**, 1119-1125.
70. S. Scheiner, R. Wysokiński, M. Michalczyk and W. Zierkiewicz, *J. Phys. Chem. A*, 2020, **124**, 4998-5006.
71. R. Wysokiński, W. Zierkiewicz, M. Michalczyk and S. Scheiner, *J. Phys. Chem. A*, 2020, **124**, 2046-2056.
72. S. Scheiner, M. Michalczyk, R. Wysokiński and W. Zierkiewicz, *Chem. Phys.*, 2020, **530**, 110590.
73. A. Grabarz, M. Michalczyk, W. Zierkiewicz and S. Scheiner, *ChemPhysChem.*, 2020, **21**, 1934-1944.
74. S. Scheiner, *Phys. Chem. Chem. Phys.*, 2020, **22**, 16606-16614.
75. A. Franconetti and A. Frontera, *Dalton Trans.*, 2019, **48**, 11208-11216.
76. Q.-Z. Li, H.-Y. Zhuo, H.-B. Li, Z.-B. Liu, W.-Z. Li and J.-B. Cheng, *J. Phys. Chem. A*, 2015, **119**, 2217-2224.
77. M. Michalczyk, W. Zierkiewicz, R. Wysokiński and S. Scheiner, *Molecules*, 2019, **24**, 3329.
78. J. Lu and S. Scheiner, *Molecules*, 2019, **24**, 2822.
79. J. Lu and S. Scheiner, *J. Phys. Chem. A*, 2020, **124**, 7716-7725.
80. S. A. Southern and D. L. Bryce, *J. Phys. Chem. A*, 2015, **119**, 11891-11899.
81. V. Kumar, C. Rodrigue and D. L. Bryce, *Cryst. Growth Des.*, 2020, **20**, 2027-2034.
82. J. E. Del Bene, I. Alkorta and J. Elguero, *Chem. Phys. Lett.*, 2016, **655–656**, 115-119.
83. Y. Chen, L. Yao and F. Wang, *J. Mol. Model.*, 2019, **25**, 351.
84. W. Dong, Q. Li and S. Scheiner, *Molecules*, 2018, **23**, 1681.
85. S. Scheiner, *J. Phys. Chem. A*, 2021, **125**, 308-316.
86. M. Michalczyk, W. Zierkiewicz, R. Wysokiński and S. Scheiner, *ChemPhysChem.*, 2019, **20**, 959-966.
87. S. P. Gnanasekar and E. Arunan, *J. Phys. Chem. A*, 2019, **123**, 1168-1176.
88. G. Mahmoudi, A. Bauza and A. Frontera, *Dalton Trans.*, 2016, **45**, 4965-4969.
89. G. Mahmoudi, A. Bauza, M. Amini, E. Molins, J. T. Mague and A. Frontera, *Dalton Trans.*, 2016, **45**, 10708-10716.
90. G. Mahmoudi, A. Bauza, A. Frontera, P. Garczarek, V. Stilinovic, A. M. Kirillov, A. Kennedy and C. Ruiz-Perez, *CrystEngComm*, 2016, **18**, 5375-5385.
91. S. Mirdya, S. Roy, S. Chatterjee, A. Bauzá, A. Frontera and S. Chattopadhyay, *Cryst. Growth Des.*, 2019, **19**, 5869-5881.
92. A. Bauzá, T. J. Mooibroek and A. Frontera, *The Chemical Record*, 2016, **16**, 473-487.
93. A. C. Legon, *Phys. Chem. Chem. Phys.*, 2017, **19**, 14884-14896.
94. S. J. Grabowski, *Phys. Chem. Chem. Phys.*, 2017, **19**, 29742-29759.
95. S. J. Grabowski, *Struct. Chem.*, 2019, **30**, 1141-1152.
96. S. Scheiner and J. Lu, *Chem. Eur. J.*, 2018, **24**, 8167-8177.
97. Q. Tang and Q. Li, *Comput. Theor. Chem.*, 2014, **1050**, 51-57.
98. X. Guo, Y.-W. Liu, Q.-Z. Li, W.-Z. Li and J.-B. Cheng, *Chem. Phys. Lett.*, 2015, **620**, 7-12.
99. A. Bauzá and A. Frontera, *ChemPhysChem.*, 2015, **16**, 3108-3113.

100. S. Shen, Y. Zeng, X. Li, L. Meng and X. Zhang, *Int. J. Quantum Chem.*, 2018, **118**, e25521.
101. H. Xu, J. Cheng, X. Yang, Z. Liu, W. Li and Q. Li, *ChemPhysChem.*, 2017, **18**, 2442-2450.
102. Y. Wei and Q. Li, *Mol. Phys.*, 2018, **116**, 222-230.
103. W. Dong, B. Niu, S. Liu, J. Cheng, S. Liu and Q. Li, *ChemPhysChem.*, 2019, **20**, 627-635.
104. W. Zierkiewicz, M. Michalczyk and S. Scheiner, *Molecules*, 2018, **23**, 1416.
105. J. Zhang, Q. Hu, Q. Li, S. Scheiner and S. Liu, *Int. J. Quantum Chem.*, 2019, **119**, e25910.
106. Y. Wei, Q. Li and S. Scheiner, *ChemPhysChem.*, 2018, **19**, 736-743.
107. L. M. Azofra, *Chem. Phys.*, 2015, **453–454**, 1-6.
108. I. Alkorta, J. Elguero and J. E. Del Bene, *J. Phys. Chem. A*, 2017, **121**, 8017-8025.
109. L. M. Azofra and S. Scheiner, *J. Chem. Phys.*, 2015, **142**, 034307.
110. I. Alkorta, J. Elguero and J. E. Del Bene, *ChemPhysChem.*, 2018, **19**, 1886-1894.
111. I. Alkorta and A. Legon, *Molecules*, 2018, **23**, 2250.
112. J. E. Del Bene, I. Alkorta and J. Elguero, *Chem. Phys. Lett.*, 2019, **730**, 466-471.
113. V. d. P. N. Nziko and S. Scheiner, *Phys. Chem. Chem. Phys.*, 2016, **18**, 3581-3590.
114. J. Del Bene, J. Elguero and I. Alkorta, *Molecules*, 2018, **23**, 906.
115. M. Hou, Z. Liu and Q. Li, *Int. J. Quantum Chem.*, 2020, **120**, e26251.
116. S. A. C. McDowell, *Chem. Phys. Lett.*, 2014, **598**, 1-4.
117. S. A. C. McDowell, *Phys. Chem. Chem. Phys.*, 2018, **20**, 18420-18428.
118. M. D. Esrafili, R. Nurazar and F. Mohammadian-Sabet, *Mol. Phys.*, 2015, **113**, 3703-3711.
119. M. D. Esrafili and F. Mohammadian-Sabet, *Mol. Phys.*, 2016, **114**, 83-91.
120. M. D. Esrafili and F. Mohammadian-Sabet, *Mol. Phys.*, 2016, **114**, 1528-1538.
121. M. D. Esrafili, N. Mohammadirad and M. Solimannejad, *Chem. Phys. Lett.*, 2015, **628**, 16-20.
122. M. Marín-Luna, I. Alkorta and J. Elguero, *J. Phys. Chem. A*, 2016, **120**, 648-656.
123. J. George and R. Dronskowski, *J. Phys. Chem. A*, 2017, **121**, 1381-1387.
124. S. Yourdkhani, T. Korona and N. L. Hadipour, *J. Comput. Chem.*, 2015, **36**, 2412-2428.
125. C. Martín-Fernández, M. M. Montero-Campillo, I. Alkorta and J. Elguero, *Mol. Phys.*, 2018, **116**, 1539-1550.
126. A. Gholipour, *Struct. Chem.*, 2018, **29**, 1255-1263.
127. L. Wang, X. Li, Y. Zeng, L. Meng and X. Zhang, *Struct. Chem.*, 2019, **30**, 1301-1313.
128. M. Vatanparast, E. Parvini and A. Bahadori, *Mol. Phys.*, 2016, **114**, 1478-1484.
129. C. Martín-Fernández, M. M. Montero-Campillo, I. Alkorta and J. Elguero, *J. Phys. Chem. A*, 2017, **121**, 7424-7431.
130. M. Hou, Y. Zhu, Q. Li and S. Scheiner, *ChemPhysChem.*, 2020, **21**, 212-219.
131. M. D. Esrafili, S. Asadollahi and P. Mousavian, *Chem. Phys. Lett.*, 2018, **691**, 394-400.
132. M. Esrafili and P. Mousavian, *Molecules*, 2018, **23**, 2642.
133. D. Sethio, V. Oliveira and E. Kraka, *Molecules*, 2018, **23**, 2763.
134. S. Scheiner, *J. Phys. Chem. A*, 2017, **121**, 3606-3615.
135. S. Scheiner, *Faraday Disc.*, 2017, **203**, 213-226.
136. S. Scheiner, *Molecules*, 2018, **23**, 1147-1155.
137. S. Scheiner, *Molecules*, 2019, **24**, 227.

138. M. Marín-Luna, I. Alkorta and J. Elguero, *J. Organomet. Chem.*, 2015, **794**, 206-215.
139. Z. Zhang, L. Wang and X. Xuan, *New J. Chem.*, 2017, **41**, 42-46.
140. D. P. Devore, T. L. Ellington and K. L. Shuford, *J. Phys. Chem. A*, 2020, **124**, 10817-10825.
141. Q. Zhao, *J. Mol. Model.*, 2020, **26**, 329.
142. Y. Hong, Y. Lu, Z. Zhu, Z. Xu and H. Liu, *Chem. Phys. Lett.*, 2020, **745**, 137270.
143. J. Yang, Q. Yu, F.-L. Yang, K. Lu, C.-X. Yan, W. Dou, L. Yang and P.-P. Zhou, *New J. Chem.*, 2020, **44**, 2328-2338.
144. T. Tondro and H. Roohi, *Journal of Chemical Sciences*, 2019, **132**, 18.
145. Y. Wang, Y. Zeng, X. Li, L. Meng and X. Zhang, *Struct. Chem.*, 2016, **27**, 1427-1437.
146. M. Saberinasab, S. Salehzadeh and M. Solimannejad, *Comput. Theor. Chem.*, 2016, **1092**, 41-46.
147. L. Spada, Q. Gou, Y. Geboes, W. A. Herrebout, S. Melandri and W. Caminati, *J. Phys. Chem. A*, 2016, **120**, 4939-4943.
148. R. Shukla and D. Chopra, *Phys. Chem. Chem. Phys.*, 2016, **18**, 13820-13829.
149. W. Li, Y. Zeng, X. Li, Z. Sun and L. Meng, *J. Comput. Chem.*, 2015, **36**, 1349-1358.
150. G. Sanchez-Sanz, C. Trujillo, I. Alkorta and J. Elguero, *Phys. Chem. Chem. Phys.*, 2014, **16**, 15900-15909.
151. Y. Chen, L. Yao and X. Lin, *Comput. Theor. Chem.*, 2014, **1036**, 44-50.
152. M. D. Esrafili, P. Fatehi and M. Solimannejad, *Comput. Theor. Chem.*, 2014, **1034**, 1-6.
153. D. Hauchecorne and W. A. Herrebout, *J. Phys. Chem. A*, 2013, **117**, 11548-11557.
154. Y. Gu, T. Kar and S. Scheiner, *J. Mol. Struct.*, 2000, **552**, 17-31.
155. U. Adhikari and S. Scheiner, *J. Chem. Phys.*, 2011, **135**, 184306.
156. V. d. P. N. Nziko and S. Scheiner, *J. Phys. Chem. A*, 2014, **118**, 10849-10856.
157. P. J. Costa, *Physical Science Reviews*, 2017, 20170136.
158. Y. Geboes, F. D. Proft and W. A. Herrebout, *J. Phys. Chem. A*, 2015, **119**, 5597-5606.
159. A. E. Kerdawy, J. S. Murray, P. Politzer, P. Bleiziffer, A. Heßelmann, A. Görling and T. Clark, *J. Chem. Theory Comput.*, 2013, **9**, 2264-2275.

Table 1. Binding energies ($-E_b$, kcal/mol) between NH_3 and indicated Lewis acid, computed at MP2/aug-cc-pVDZ level, with counterpoise corrections included.

T	TH_4	FTH_3	F_3TH	F_4T
	σ_H[a]	σ_F[b]	σ_H	σ_F
C	-	1.84	-	0.82
Si	1.66	5.49	4.75	10.59
Ge	1.48	5.84	8.68	16.77
Sn	2.44	8.51	18.20	25.53

[a]position opposite to H, [b]position opposite to F

Table 2. Maximum in MEP on 0.001 au isodensity surface (kcal/mol) of indicated monomer at MP2/aug-cc-pVDZ level (aug-cc-pVDZ(PP) for Sn). Maximum lies opposite F for FTH_3 and H for F_3TH.

T	TH_4	FTH_3	F_3TH	F_4T
	σ_H	σ_F	σ_H	σ_F
C	-	21.3	10.1	25.0
Si	19.4	41.1	34.8	50.0
Ge	17.8	45.1	34.2	58.8
Sn	24.3	53.7	45.4	74.5

Table 3. Angular deformation within monomers caused by complexation with NH_3

T	TH_4	FTH_3	F_3TH	F_4T
	$\Delta\theta$(X-T-Y), deg			
C	-	0.1	-	-0.6
Si	-1.4	-4.9	-12.6	-12.7
Ge	-1.2	-4.6	-12.9	-12.5
Sn	-2.5	-5.3	-12.0	-11.0
	E_{def}, kcal/mol			
C	-	0.02	-	0.06
Si	0.14	1.93	21.38	20.78
Ge	0.11	1.51	18.99	16.61
Sn	0.37	1.77	12.50	9.62

Table 4. Equilibrium R(Si··N) intermolecular distance and energetics (kcal/mol) in complexes of $FSiR_3$ with NH_3, at MP2/aug-cc-pVDZ level (aug-cc-pVDZ(PP) for I), with counterpoise corrections included.

$FSiR_3$	R, Å	E_{int}	E_{def}	E_b
$FSiH_3$	2.557	-7.42	1.93	-5.49
$FSiMe_3$[a]	3.753	-2.37	0.13	-2.24
$FSiMe_2(CF_3)_1$	2.392	-13.15	11.04	-2.11
$FSiMe_1(CF_3)_2$	2.208	-24.97	15.75	-9.22
$FSi(CF_3)_3$	2.116	-35.55	17.35	-18.20
$FSiIso_3$ a	3.091	-2.26	2.50	+0.24
b	2.499	-7.36	14.16	+6.80
$FSiIso_2(CF_3)_1$	2.384	-12.98	10.28	-2.70
$FSiTb_3$	2.519	-6.61	17.41	+10.80
$FSiCl_3$	2.068	-25.34	19.89	-5.45
$FSiBr_3$	2.078	-22.61	17.89	-4.73
$FSiI_3$	2.130	-18.09	14.78	-3.31

[a] primarily stabilized by CH··N

Table 5. Equilibrium R(T··N) intermolecular distance and energetics (kcal/mol) in complexes of FTR_3 with NH_3.

FTR_3	R, Å	E_{int}	E_{def}	E_b
$FGeH_3$	2.627	-7.33	1.49	-5.84
$FGeMe_3$	2.775	-1.77	0.41	-1.36
$FGeIso_3$	2.823	-6.02	2.38	-3.64
$FGeTb_3$	2.670	-6.08	12.71	+6.63
$FSnTb_3$	2.653	-9.84	6.42	-3.42
$FPbTb_3$	2.851	-7.66	2.89	-4.77

Table 6. Energetics (kcal/mol) of tetrel-bonded complexes involving TF_4, at MP2/aug-cc-pVDZ level (aug-cc-pVDZ(PP) for Sn)

FTR_3	E_{int}	E_{def}	E_b
HCN···SiF_4	-2.63	0.44	-2.19
HCN···GeF_4	-6.76	3.41	-3.35
HCN···SnF_4	-16.99	6.22	-10.77
pyrazine···SiF_4	-20.80	16.79	-4.01
pyrazine ···GeF_4	-29.33	17.45	-11.88
pyrazine···SnF_4	-34.50	11.62	-22.88
NH_3···SiF_4	-26.38	20.29	-6.09
NH_3···GeF_4	-31.23	16.90	-14.33
NH_3···SnF_4	-35.29	10.26	-25.03

Table 7. Energetics (kcal/mol) of tetrel-bonded complexes and MEP maxima on 0.001 au isodensity surface of TF_4 monomers, at MP2/aug-cc-pVDZ level (aug-cc-pVDZ(PP) for Sn)

FTR_3	$E_{int}(f)^a$	$E_{int}(f)$-$E_{int}(opt)^b$	$V_{max}(f)^a$	$V_{max}(opt)^b$
HCN···SiF_4	-1.89	0.74	41.3	48.2
HCN···GeF_4	-2.64	5.12	50.9	73.1
HCN···SnF_4	-5.44	11.55	70.1	102.4
pyrazine···SiF_4	-3.25	17.55	41.3	88.3
pyrazine ···GeF_4	-4.93	24.40	50.9	98.0
pyrazine···SnF_4	-11.17	23.33	70.1	109.7
NH_3···SiF_4	-2.98	23.40	41.3	92.3
NH_3···GeF_4	-4.68	26.55	50.9	97.2
NH_3···SnF_4	-12.26	23.03	70.1	108.0

[a]TF_4 frozen in its optimized monomer geometry

[b]TF_4 in geometry optimized within complex

Table 8. Binding energies (kcal/mol) for complexes between NMA and indicated Lewis acid, computed at MP2/aug-cc-pVDZ level

	C··O TB	CH··O HB	SH··O HB	CS··O YB	FS··O YB
$FHSCH_3^+$	17.31	21.17	34.09	23.43	39.03
$CH_3SH_2^+$	16.03	18.33	29.24	21.95	-
$(CH_3)_3S^+$	13.72	16.30[a] 20.55[b]	-	19.81	-
$FSCH_3$	2.50	3.29	-	2.71	6.40
CH_3SH	1.90	1.67	4.12	1.14	-

[a]single linear CH··O

[b]trifurcated: 3 different CH_3 groups

Table 9. Interaction energies, changes in internal stretching frequencies and NMR chemical shielding caused by complexation , calculated at the MP2/aug-cc-pVDZ level (aug-cc-pVDZ(PP) for Sb, Te, Sn and I)

	E_{int}, kcal/mol	Δν, cm^{-1}		Δσ,ppm				
HB		X-H	C=O	H	X	O	C	N
FH···NMA	-12.68	-729	-30	-6.9	-19.5	34.4	-6.3	-5.1
ClH···NMA	-10.14	-695	-50	-9.5	-1.0	20.0	-6.0	-5.4
BrH···NMA	-9.22	-705	-75	-10.6	35.8	15.4	-6.2	-5.6
IH···NMA	-7.23	-606	-169	-11.2	175.7	7.0	-6.1	-5.7
XB		F-X		X	F			
FCl···NMA	-9.69	-103	-45	239.3	-139.2	28.4	-5.4	-5.4
FBr···NMA	-13.34	-80	-55	929.2	-208.8	46.5	-7.1	-7.7
FI···NMA	-15.75	-58	-55	2196.7	-296.2	62.6	-7.8	-9.9
YB		F-Y		Y	F			
HFS···NMA	-8.90	-71	-28	141.2	-112.0	28.1	-4.0	-4.6
HFSe···NMA	-11.18	-64	-36	521.2	-151.9	38.8	-4.9	-6.5
HFTe···NMA	-13.82	-56	-49	1310.8	-193.1	49.4	-7.6	-8.4
ZB		F-Z		Z	F			
H_2FP···NMA	-7.40	-58	-24	40.0	-62.2	22.0	-4.0	-4.3
H_2FAs···NMA	-8.65	-54	-29	107.6	-71.1	27.5	-4.5	-5.5
H_2FSb···NMA	-11.40	-51	-40	283.9	-80.6	35.2	-6.3	-7.2
TB		F-T		T	F			
H_3FSi···NMA	-7.70	-57	-23	17.3	-42.5	17.0	-4.0	-4.5
H_3FGe···NMA	-8.37	-57	-25	42.5	-47.3	19.8	-4.3	-5.2
H_3FSn···NMA	-12.22	-50	-35	127.0	-53.0	29.4	-5.8	-7.6

Table 10. Binding energy, intermolecular distance, and orientation angle in complexes with NH_3, calculated at MP2/aug-cc-pVTZ level

	E_b, kcal/mol	R, Å	θ(R-A··N), degs
	H-H_nA		
HBr	-1.86	3.174	179.9
H(H)Se	-2.15	3.206	162.7
H(H_2)As	-1.68	3.235	162.6
H(H_3)Ge	-1.53	3.276	180.0
	Me-H_nA		
MeBr	-1.19	3.233	160.4
Me(H)Se	-1.87	3.234	166.6
Me(H_2)As	-1.48	3.268	168.5
Me(H_3)Ge	-1.17	3.329	179.7
	H-F_nA		
H(F)Se	-3.32	3.023	161.6
H(F_2)As	-4.09	2.882	155.0
H(F_3)Ge	-8.37	2.101	180.0
	Me-F_nA		
Me(F)Se	-2.74	3.114	162.7
Me(F_2)As	-3.26	3.021	155.3
Me(F_3)Ge	-6.16	2.115	180.0

Table 11. Interaction energies and intermolecular separations when NH_3 is added to either the T or X atom of TF_3X at the M06-2X/aug-cc-pVDZ level of theory (aug-cc-pVDZ(PP) for Sn and I)

		-E_{int}, kcal/mol		R, Å	
T	X	TB	XB	TB	XB
C	Cl	1.35	2.74	3.221	2.983
	Br	1.39	4.06	3.238	3.018
	I	1.15	6.61	3.226	2.979
Si	Cl	35.99	1.67	2.043	3.187
	Br	36.70	2.64	2.040	3.191
	I	36.92	4.23	2.042	3.229
Ge	Cl	35.59	2.18	2.124	3.138
	Br	35.57	3.48	2.124	3.120
	I	34.85	5.62	2.129	3.104
Sn	Cl	37.75	2.08	2.281	3.108
	Br	37.14	3.58	2.284	3.106
	I	36.33	5.95	2.284	3.093

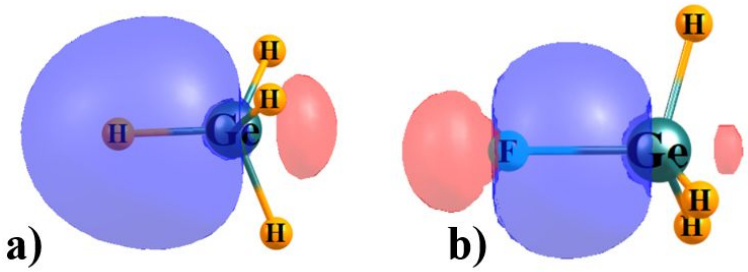

Fig. 1. σ(Ge-X) bonding orbital from NBO localization scheme for a) GeH_4 and b) $GeFH_3$. Red and blue colors indicate opposite phase of the orbital.

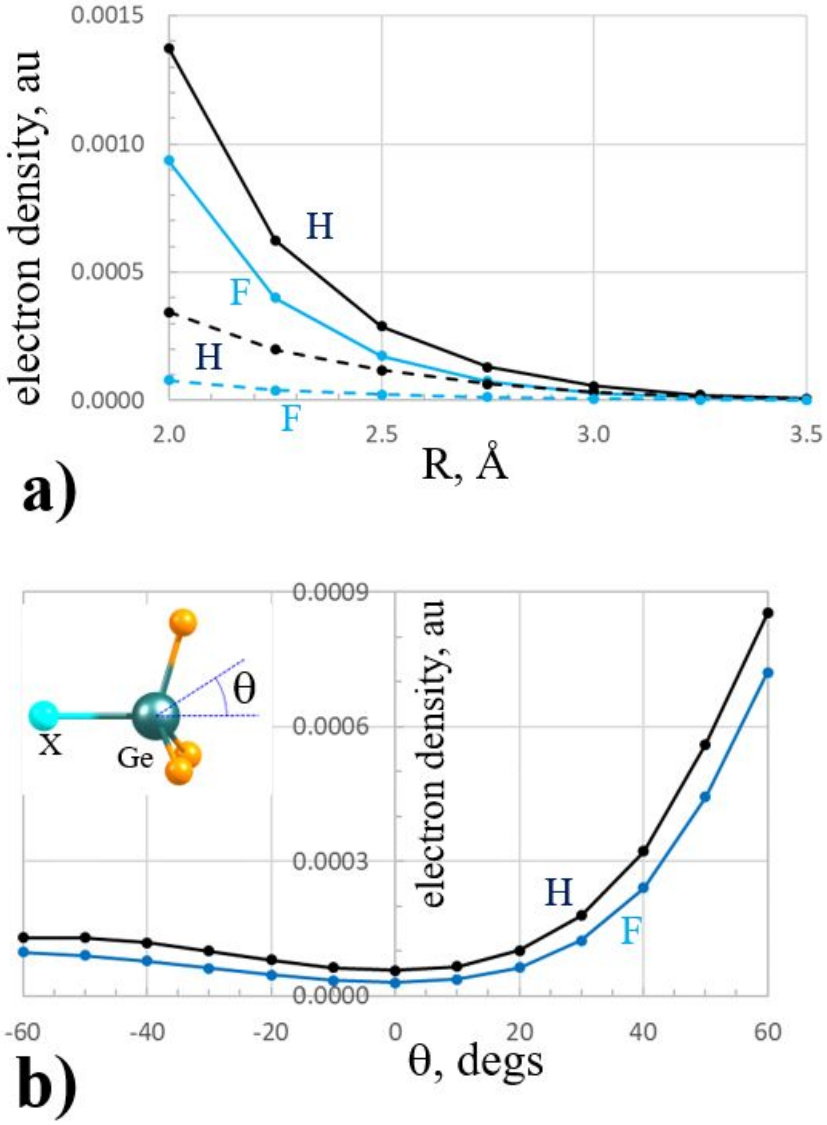

Fig 2. Broken lines in a) indicate the electron density associated with σ(Ge-X) bonding orbital ($2\varphi^2$) along the extension of the X-Ge axis. Solid lines refer to the total electron density. b) Total electron density of GeH_4 and $GeFH_3$, as a function of θ which measures the deviation from the extension of the X-Ge covalent bond, at a distance of 3 Å from Ge. Black and blue curves refer respectively to GeH_4 and $GeFH_3$.

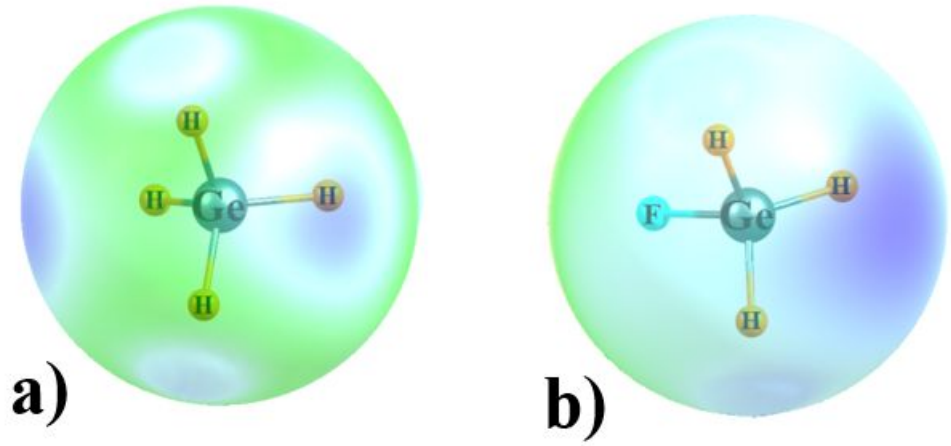

Fig. 3. Molecular electrostatic potentials surrounding a) GeH_4 and b) $GeFH_3$. Red and blue colors indicate minima and maxima, respectively, ±0.01 au for GeH_4 and ±0.03 au for $GeFH_3$. Surface represents 1.5 x atomic vdW radii.

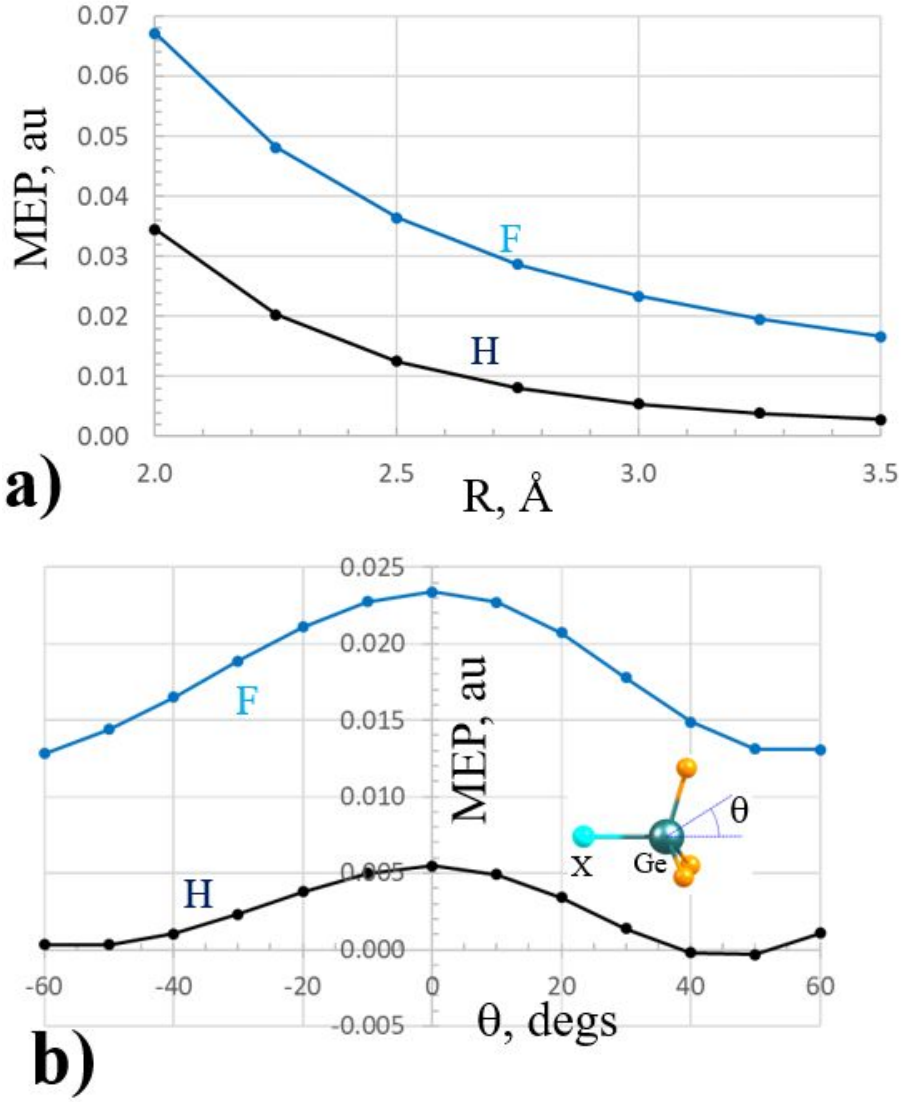

Fig. 4 MEP a) along the extension of the X-Ge axis and b) at a constant distance of 3 Å from Ge atom. Black and blue curves refer respectively to GeH_4 and $GeFH_3$.

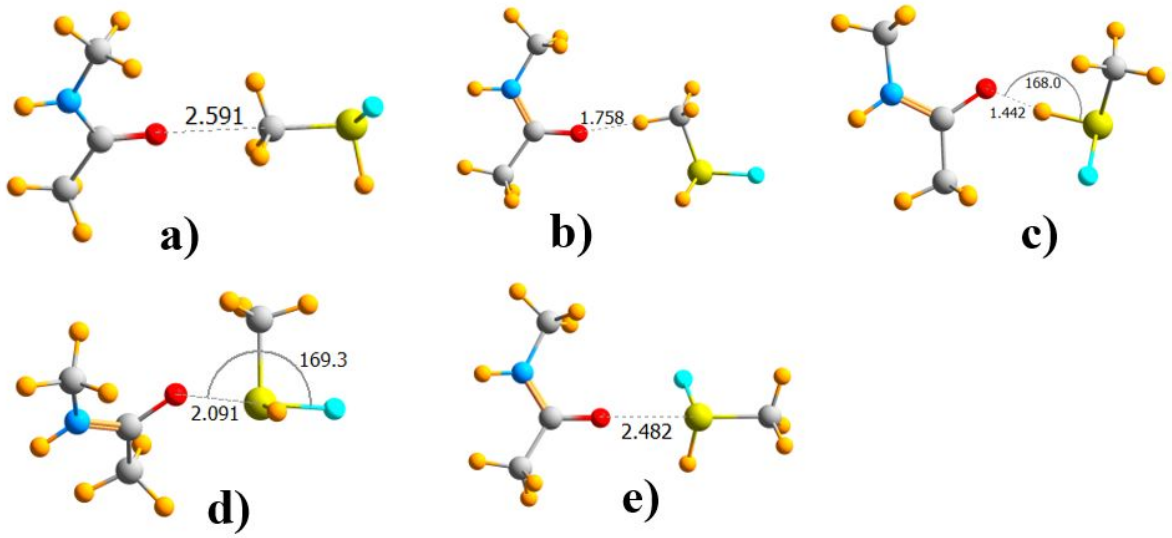

Fig 5 MP2/aug-cc-pVDZ optimized geometries of complexes of NMA with a) $FHSCH_3^+$. Distances in Å, angles in degs.

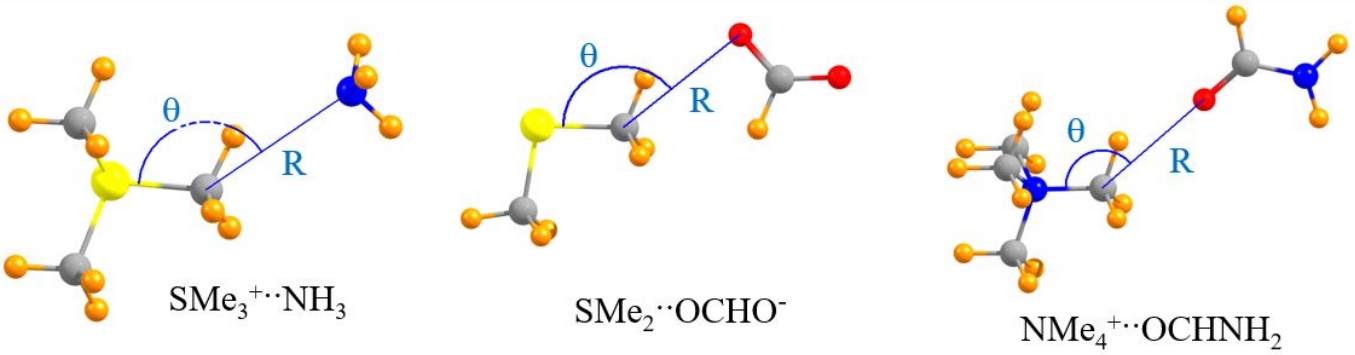

Fig 6. Molecular diagrams of three of the systems examined, defining intermolecular distance R and angle θ.

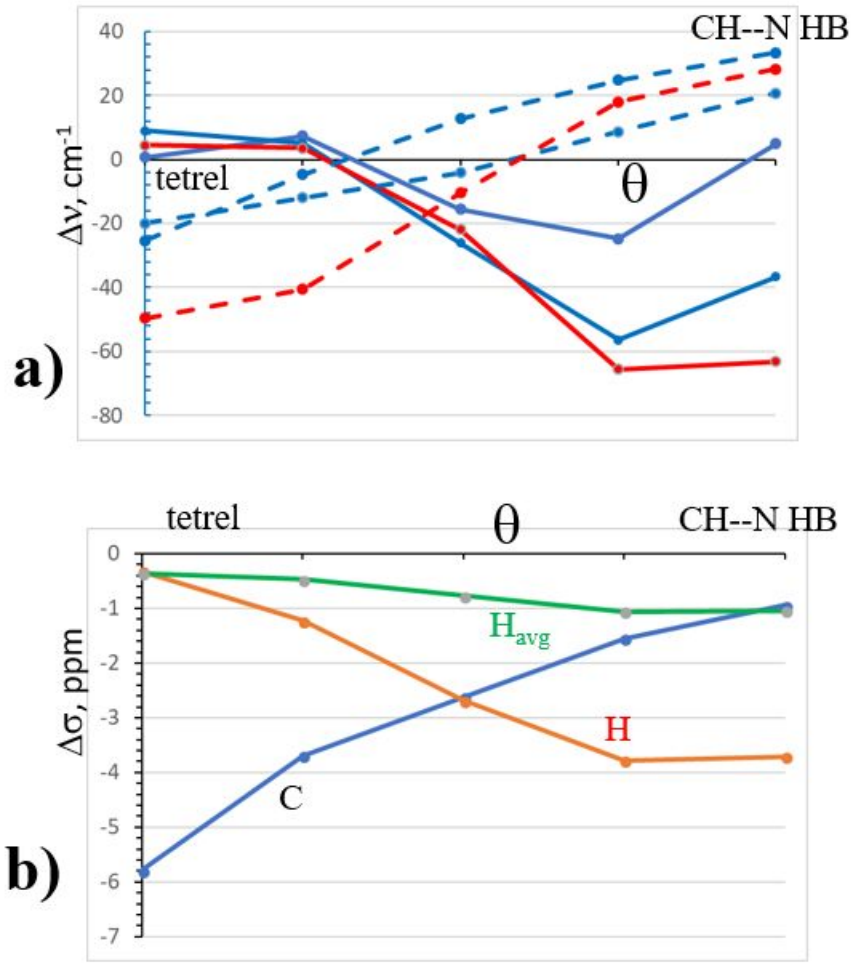

Fig 7. Changes in spectra of $SMe_3^{+}\cdot\cdot NH_3$ caused by interaction. a) vibrational frequencies of methyl group. Solid curves refer to stretching modes and bending modes are indicated by broken curves. Blue and red colors respectively represent asymmetric and symmetric motions. b) changes in chemical shielding. Tetrel-bonding configuration (θ=180º) on the left and CH··O/N H-bond (θ~110º) on the right.

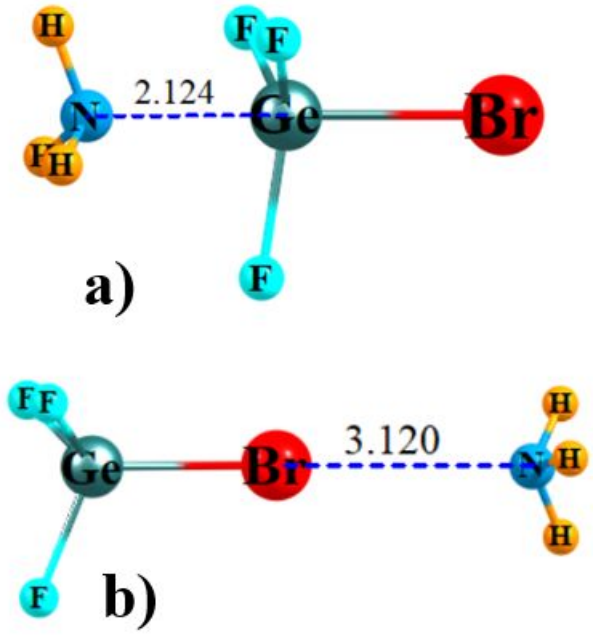

Fig 8. a) Tetrel-bonded and b) halogen-bonded complexes of GeF_3Br with NH_3. Distances in Å.